

Impacts of Vertical Greenery on Outdoor Thermal Comfort and Carbon Emission Reduction at the Urban Scale in Turin, Italy

Original

Impacts of Vertical Greenery on Outdoor Thermal Comfort and Carbon Emission Reduction at the Urban Scale in Turin, Italy / Dehghan Lotfabad, Amir; Morteza Hosseini, Seyed; Dabove, Paolo; Heiranipour, Milad; Sommese, Francesco. - In: BUILDINGS. - ISSN 2075-5309. - 15:3(2025), pp. 1-31. [10.3390/buildings15030450]

Availability:

This version is available at: 11583/3003576 since: 2025-10-01T16:43:07Z

Publisher:

Multidisciplinary Digital Publishing Institute (MDPI)

Published

DOI:10.3390/buildings15030450

Terms of use:




This article is made available under terms and conditions as specified in the corresponding bibliographic description in the repository

Publisher copyright

(Article begins on next page)

Article

Impacts of Vertical Greenery on Outdoor Thermal Comfort and Carbon Emission Reduction at the Urban Scale in Turin, Italy

Amir Dehghan Lotfabad ¹, Seyed Morteza Hosseini ^{2,*} , Paolo Dabove ¹ , Milad Heiranipour ³ and Francesco Sommese ⁴ 

¹ Department of Environment, Land and Infrastructure Engineering, Politecnico di Torino, Corso Duca degli Abruzzi, 24, 10129 Turin, Italy; amir.dehghanlotfabad@studenti.polito.it (A.D.L.); paolo.dabove@polito.it (P.D.)

² Department of Architecture, Design & Media Technology, Aalborg University Copenhagen, A.C. Meyers Vænge 15, 2450 Copenhagen SV, Denmark

³ Department of Energy, Politecnico di Torino, Corso Duca degli Abruzzi, 24, 10129 Turin, Italy; milad.heiranipour@polito.it

⁴ Department of Civil, Building and Environmental Engineering, University of Naples Federico II, P.le Vincenzo Tecchio, 80, 80125 Naples, Italy; francesco.sommese@unina.it

* Correspondence: smho@create.aau.dk

Abstract: Urban heat islands (UHIs) increase urban warming and reduce outdoor thermal comfort due to changing surface characteristics and climate change. This study investigates the role of green walls (GWs) in mitigating UHI, improving outdoor thermal comfort, and reducing carbon emissions under current and future (2050) scenarios. Focusing on Via della Consolata, Turin, Italy, the study combines remote sensing for UHI detection and numerical simulations for thermal analysis during seasonal extremes. The results show that GWs slightly reduce air temperatures, with a maximum decrease of 1.6 °C in winter (2050), and have cooling effects on mean radiant temperature (up to 2.27 °C) during peak summer solar radiation. GWs also improve outdoor comfort, reducing the Universal Thermal Climate Index by 0.55 °C in the summer of 2050. The energy analysis shows that summer carbon emission intensity is reduced by 31%, despite winter heating demand increasing emissions by 45%. The study highlights the potential of GWs in urban climate adaptation, particularly in dense urban environments with low sky view factors. Seasonal optimization is crucial to balance cooling and heating energy demand. As cities face rising temperatures and heat waves, the integration of GWs offers a sustainable strategy to improve microclimate, reduce carbon emissions, and mitigate the effects of UHI.

Keywords: air temperature; climate change; green wall; mean radiant temperature; urban heat island



Academic Editor: Apple L.S. Chan

Received: 5 January 2025

Revised: 26 January 2025

Accepted: 27 January 2025

Published: 31 January 2025

Citation: Dehghan Lotfabad, A.; Hosseini, S.M.; Dabove, P.; Heiranipour, M.; Sommese, F. Impacts of Vertical Greenery on Outdoor Thermal Comfort and Carbon Emission Reduction at the Urban Scale in Turin, Italy. *Buildings* **2025**, *15*, 450. <https://doi.org/10.3390/buildings15030450>

Copyright: © 2025 by the authors. Licensee MDPI, Basel, Switzerland. This article is an open access article distributed under the terms and conditions of the Creative Commons Attribution (CC BY) license (<https://creativecommons.org/licenses/by/4.0/>).

1. Introduction

1.1. Background

In today's world, over half of the world's population (54 percent) lives in urban areas. The coming decades will bring further profound changes to the size and spatial distribution of the global population. The world's population in 2050 is projected to be 66 percent urban dwellers, with the global urban population projected to grow by 2.5 billion urban dwellers between 2014 and 2050 [1]. Urbanization can cause problems for city inhabitants. One of the more prominent problems is the UHI effect of the urban canopy layer, which can also increase energy consumption [2]. The UHI effect is responsible for having higher air and surface temperature [3]. On a sunny day, solar irradiation will heat up the surfaces during

the day, while at night, the temperature in the environment will be lower, and the surfaces will exchange the absorbed heat with their colder surroundings. The surface temperature is the main parameter affecting the mean radiant temperature (T_{mrt}) and consequently the universal thermal climate index (UTCI), alongside relative humidity and wind speed. Understanding the factors influencing the UHI effect is crucial for better use of urban heat reduction strategies and solutions. The most utilized research methods in this area of research were numerical model simulation, followed by mobile or stationary ground-based measurements and remote sensing. While satellite-based observations focus on surface temperature on a mesoscale, numerical simulations and field measurements provide further environmental parameters that allow for human thermal comfort analysis at the pedestrian level and consider the air temperature instead of the surface temperature, which is essential to predict the effect of heat events on human health and energy consumption [4–6]. It is also known that the diurnal profiles of surface urban heat islands (SUHIs) differ from those of canopy UHIs. Large SUHI generally occurs during the daytime, while large canopy UHI generally occurs at night, and therefore spatial assessment of canopy UHI through remote sensing techniques at a fine scale may introduce estimation error [7].

1.2. Examining the Factors Influencing UHI

The studies with statistical models such as stepwise multiple linear regression (SMLR), XGBoost, bivariate and multivariate analysis, and Pearson correlation analysis highlight the effects of urban morphology, building geometries, and surface properties on the UHI. Findings consistently demonstrate a strong correlation between urban morphology and UHI effects, particularly in densely built areas with high-rise structures. The UHI effect is influenced by several key morphological parameters, including building height, density, size, aspect ratio, sky view factor (SVF), area, and orientation [6,8]. Of these factors, orientation is unique in its effects on energy use intensity and thermal comfort [9,10].

Building height and volume would increase nighttime SUHI as they store heat during the day and release it at night, and density increases daytime SUHI by elevating heat absorption and increasing heat retention in cities. Conversely, wider urban canyons could reduce SUHI by allowing better air circulation as wind speed reduces nighttime SUHI [11]. Findings show that the three main morphological parameters affecting UHI are SVF, street length (SL), and pervious surface fraction. Two main parameters of the increase in the total length of the streets in the site and the decrease in the SVF, which has a negative correlation with the ratio of mean building height to mean street width in the sample site (H/W), would exacerbate the SUHI [7]. SVF ranges from 0 to a maximum of 1, which is completely open to the sky and is defined as the percentage of free sky at a specific location [12,13]. A moderate-to-high SVF can mitigate UHI, whereas extremely high SVF levels intensify it [14]. In a simulation study with Envi-met [15] of the effect of the built environment (H/W), urban greenery, and SVF on thermal comfort, a regression analysis showed that the effect of SVF on air temperature was smallest. In contrast, its effect on surface temperature and consequently T_{mrt} , as an important parameter influencing UTCI [16], is the largest. A 0.1 unit increase in SVF led to an increase of 1.6 °C and 2.4 °C in air temperature and 17.9 °C and 16.7 °C in T_{mrt} within N-S and E-W streets, respectively. It also proves the effect of the orientation of buildings, to be considered by designers for the future development of cities [17]. Ref. [18] concerned with the best urban morphology parameters on air temperature, solar radiation, wind speed, T_{mrt} , and Physiological Equivalent Temperature (PET) in three different sites in Nanjing, China, without considering anthropogenic heat emissions. They found that, in general, by increasing SVF, the air temperature would increase, and increasing building area is not the main cause of the increase in air temperature. However, the variation in T_{mrt} was greater than air temperature. The correlation between T_{mrt} and SVF is different between

day and night, with a positive correlation in daytime and a negative correlation in nighttime. The T_{mrt} correlates positively with the distance between buildings, gaining solar radiation in the daytime, and has a negative correlation with building heights. They also found areas with lower SVF, lower distance between buildings, lower solar radiation, and consequently lower T_{mrt} and better PET [11]. Also mentioned other factors influencing SUHI and indicated that, instead of urban morphology, climate background has a weak correlation with SUHI, and the relationship between different climate zones and geographical locations is varied. Conversely, surface properties, such as enhanced vegetation index, are the most critical factor for mitigating daytime heat, since urbanization causes a significant reduction in greenness in urban areas, which reduces the evapotranspiration capacity within the city and subsequently enhances SUHI intensities.

1.3. Urban Heat Island Mitigation Scenarios and State-of-the-Art

One UHI mitigation strategy for existing urban context without configuration in the urban morphology and orientation is the modification and incorporation of sustainable building materials into the built environment by changing the albedo of surfaces such as pavements and facades with high thermal effects materials and painting materials to be bright and reflective in the summer [19]. However, Ref. [20] gave suggestions that changing albedo solely would not improve thermal comfort enough in extreme events and recommended using additional strategies such as shading and evaporative cooling, especially in areas with low aspect ratios. In this case, urban areas around the world are increasingly investing in networks of urban forests, gardens, and other forms of green infrastructure (Table 1) such as trees, which (irrespective of configuration) can reduce thermal sensation from “Very Hot” conditions to “Hot”, irrespective of the street canyon’s aspect ratio [21], green roofs, and vertical greenery systems (VGSs) for their benefits in improving a building’s thermal and acoustic insulation, reducing the urban heat island effect, increasing urban biodiversity, and improving air quality [22,23], and reducing cooling energy demand, which consequently reduces CO₂ emissions in summer months [24]. Climate change also presents opportunities to promote urban green infrastructure [25], which, as a climatic background, is considered one of the factors affecting UHI. It is important to understand how to intervene in particularly compact and dense urban structures where there is not enough space to implement nature-based solutions [26]. In densely urbanized areas, buildings’ surfaces (i.e., façades and rooftops) can offer room for the installation of vegetation [27]. One of the well-known green initiatives implemented in dense urban environments is vertical greening due to its small footprint and ability to cover a large surface area as well as lower installation costs [3,28]. It has also been concluded that in a densely urbanized area characterized by high-rising buildings, green walls are more beneficial in mitigating UHI than extensive green roofs (EGRs), which have a negligible effect on urban warming. Using plants is more beneficial than other devices on facades, as the temperature of the leaves is lower than other materials. Around 60% of solar radiation absorbed by plants transforms into latent heat and sensible heat by evaporative cooling, provided by evapotranspiration from the plants and the substrate [29–31]. Consequently, it can reduce the fluctuations of surface temperature, air temperature, and relative humidity, alongside the amount of particulate matter on the walls, by reducing the risk of most common degradation mechanisms induced by salts and frost in historic building materials [3] such as the once in Italy. Furthermore, the study in Turin, Italy, shows that these mitigation strategies are more effective in mitigating summer UHI when installed in canyons parallel to the main wind direction than in perpendicular ones. It also shows that it is necessary to increase plant watering to promote the stomatal opening for adapting to

UHI during summer heat waves [27]. It must be mentioned that more than three hours of direct sunlight is necessary for the growth of vegetation [32].

Table 1. Table of state-of-the-art. *cei*: carbon emission intensity; *AP*: air pollutants; *EC*: energy consumption; *HBvc*: heat balance of the vegetation canopy; *ILP*: indoor lighting performance; *LW*: longwave radiation; *PET*: psychological equivalent temperature; *PMV*: predicted mean vote; *RH*: relative humidity; *SW*: shortwave radiation; *Ta*: air temperature; *Tf*: foliage temperature; *Tmrt*: mean radiant temperature; *To*: operative temperature; *Ts*: surface temperature; *Twbgt*: wet bulb globe temperature; *UTCI*: universal thermal climate index; *Wd*: wind direction; *Ws*: wind speed.

Scenario and/or Goals	Year	Climate	Insite Measured Parameters (Sensor Based)	Methodology	Results	cei	Future
Study on albedo configurations for walls and floors: [20] <ul style="list-style-type: none"> Low: <0.3 Medium: 0.3–0.7 High: >0.7 	2022	Csa	<i>Ta</i> ; <i>RH</i> ; <i>Ws</i> ; <i>Tmrt</i>	Validated simulation	<i>Ta</i> ; <i>Tmrt</i> ; <i>PET</i> ; <i>Ts</i>	×	×
<ul style="list-style-type: none"> Green roofs Tree planting [33] 	2023	Zone C	The data that has been used is confidential	Validated simulation	<i>EC</i> ; <i>AP</i> ; <i>Ta</i> ; <i>Tmrt</i> ; <i>LW</i>	×	×
Varying greenery coverage: [31] <ul style="list-style-type: none"> Green roofs Green façade 	2018	Af	<i>Ta</i> ; <i>RH</i> ; <i>Ws</i>	Validated simulation	<i>Ta</i> averaged	×	×
Analyzing two VGSs: [34] <ul style="list-style-type: none"> With soil With plant, soil (albedo 0.43), and high-albedo walls (0.78) positioned 0.4 m 	2023	Dwa	<i>Ta</i> ; <i>Ts</i> ; <i>Tmrt</i> ; <i>RH</i> ; <i>Ws</i>	Experimental study	<i>SW</i> ; <i>LW</i> ; <i>Tmrt</i> ; <i>Ts</i>	×	×
Vegetated green façade on reduced-scale buildings [35]	2017	Cfb	<i>Ts</i> Inside; <i>Ta</i> Inside	Experimental study	<i>Ta</i> ; <i>Ta</i> Inside; <i>Ts</i> Inside; <i>To</i>	×	×
Two VGSs technologies: [36] <ul style="list-style-type: none"> Green Walls (GWs) Vertical Forest 	2025	Csa	<i>Ta</i> ; <i>RH</i> ; <i>Ws</i> ; <i>Wd</i> ; <i>SW</i> ; <i>LW</i> ; <i>Ts</i>	Validated simulation	<i>Tmrt</i> ; <i>PET</i> ; <i>UTCI</i>	×	×
Configurations of: <ul style="list-style-type: none"> Living walls (LWs) Green façades EGRs 	2023	Cfa Csa	<i>Ta</i> ; <i>RH</i> ; <i>Wd</i> ; <i>Ws</i>	Validated simulation	<i>Ta</i>	×	×
Considering wind direction, scale, and orientations [27]							
Thermal impact of urban green systems on UHI [37]: <ul style="list-style-type: none"> Trees Living façades High albedo pavements 	2024	Cfb	Not specified	Validated simulation	<i>RH</i> ; <i>Ts</i> ; <i>Ta</i> ; <i>Tmrt</i> ; <i>PET</i>	×	✓
Thermal performance of 4 parametric green façade systems [38]	2024	Bsk	Not specified	Validated simulation	<i>EC</i> ; <i>ILP</i>	✓	×
Effect of GWs on urban microclimate [39]	2019	BWh	<i>Ta</i> ; <i>Wd</i> ; <i>Ws</i> ; <i>RH</i>	Validated simulation	<i>Ta</i> ; <i>Ta</i> Inside; <i>PMV</i> ; <i>RH</i>	×	×
Thermal balance of vegetation canopy [29]	2019	Cfa	<i>SW</i> ; <i>LW</i> ; <i>Tf</i> ; <i>Ta</i> ; <i>Ts</i> ; <i>Ws</i> ; <i>RH</i>	Experimental Study	<i>LW</i> ; <i>SW</i> ; <i>Ta</i> ; <i>Ws</i> ; <i>HBvc</i> ; <i>Ts</i> ; <i>EC</i> ; <i>To</i> ; <i>Twbgt</i>	×	×

1.4. Objectives and Contributions

From the literature, it has been concluded that urban morphology, climate background, and surface properties are the main factors amplifying the UHI effect (Figure 1), leading to increased air and surface temperatures in cities. Green facades and green roofs have been widely studied for their cooling benefits, including impacts on air temperature, *Tmrt*, outdoor comfort, and energy efficiency, particularly during summer and heat waves, as

well as in winter conditions. They conclude that vertical greenery systems have better cooling efficiency compared to horizontal surfaces such as green roofs. However, analyses of energy efficiency and outdoor comfort are limited to small-scale assessments, focusing on a single block. Additionally, they did not consider the effect of climate change and failed to evaluate how greenery can mitigate carbon emission intensity.

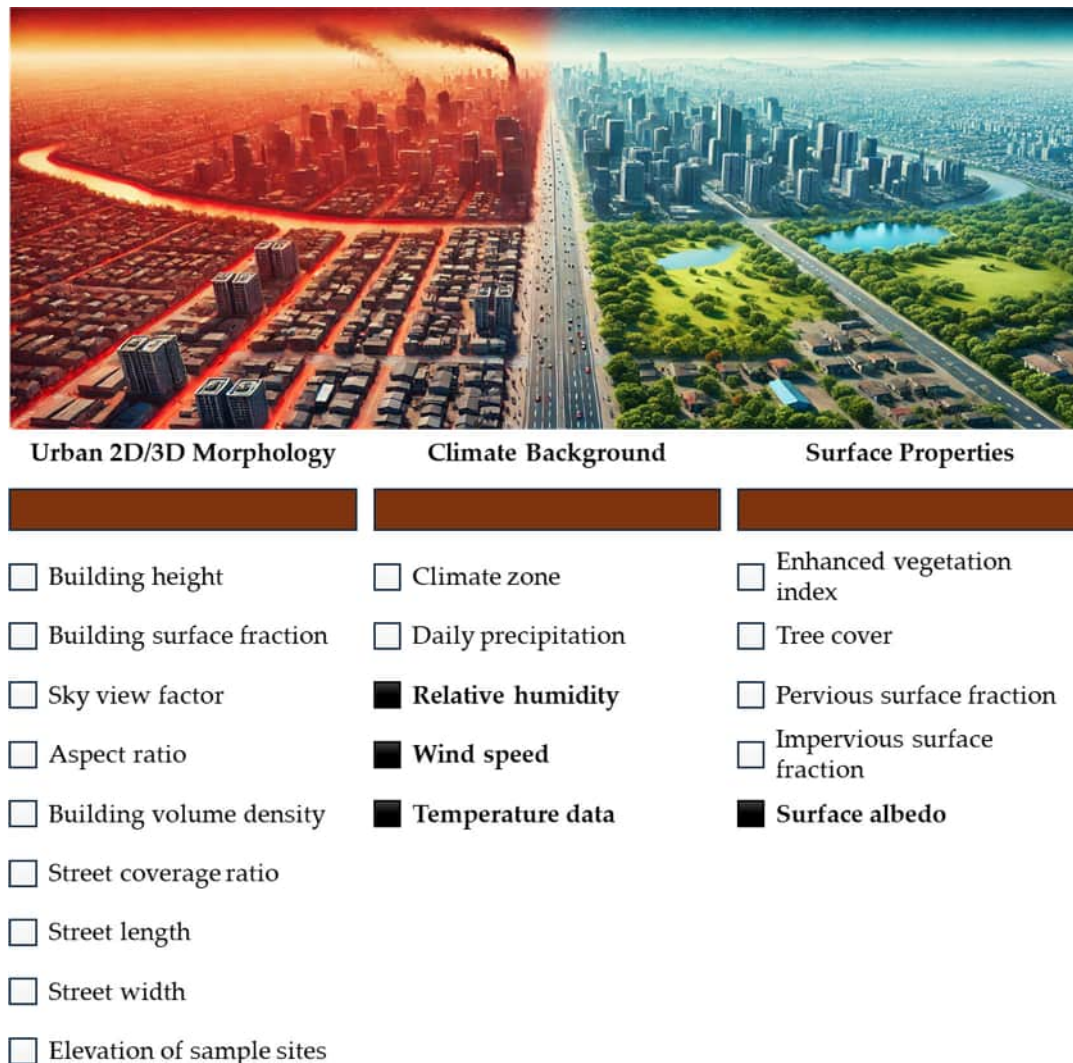


Figure 1. Drivers of urban heat islands and the scope of the study.

To fill this gap, our study aims to evaluate the effect of green walls on air temperature, T_{mrt} , and outdoor thermal comfort, as well as its contribution to reducing the (cei) of the Heating, Ventilation, and Air Conditioning (HVAC) systems under current and future climate projections. The study is conducted on the scale of a few blocks, considering all the outdoor walls are covered entirely by green walls.

2. Materials and Methods

The methodology of this study comprises two sections, as illustrated in Figure 2. The initial section is devoted to the analysis and detection of the urban area experiencing the intense SUHI effect. This is followed by the selection of the study area through the utilization of remote sensing techniques. The subsequent section involves the evaluation and simulation of the mitigation scenario of green walls.

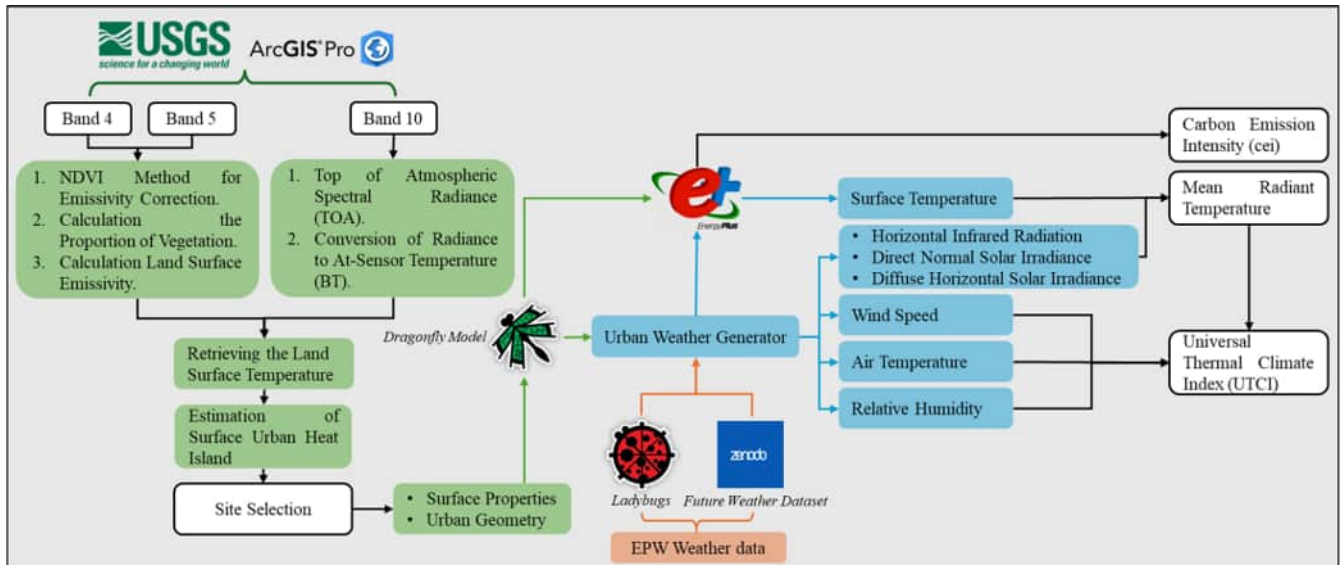


Figure 2. Flowchart of the analysis of the SHUHI and site selection along with the simulation workflow.

2.1. Data Gathering

2.1.1. Satellite Data

The surface reflectance and emittance records of the Landsat-9 satellite were utilized in this study. The three Landsat-9 bands employed in this investigation were Band 4, Band 5, and Band 10 (Table 2). It is noteworthy that Band 4, which operates within the visible spectrum, possesses extremely short wavelengths. In contrast, the remaining bands function in regions of the spectrum that are imperceptible to the human eye. Band 5, which is sensitive to near-infrared (NIR) light, was particularly insightful. This region, which is reflected at maximum by healthy plants, which are the highest natural reflectors, up to 70%, can be used for the study of ecology. Band 10 operates within the thermal infrared (TIR) spectrum, detecting emitted thermal radiation. In contrast to the measurement of air temperature by a meteorological weather station, Band 10 reports the surface temperature, which is typically significantly hotter due to the ground's greater capacity for heat absorption and retention. The Landsat-9 satellite image and associated data were retrieved on 11 July 2023 [40]. The date was selected due to its representation of both the most recent and the oldest data, which predominantly covers the Turin municipality area with minimal cloud cover.

Table 2. Landsat 9 image characteristics.

Data Type	Time	Cloud Cover	Band Number	Resolution
Landsat 9 satellite imagery "OLI_TIRS"	11 July 2023, 11:16:53.4756430Z	3.34%	Band 4—Red	30.00 (m)
			Band 5—Near-infrared (NIR)	30.00 (m)
			Band 10—Thermal infrared 1 (TIRS1)	30.00 (m)

2.1.2. Weather Data

Weather data for creating site weather conditions were retrieved from Ladybug Tools EPWmap with the hourly temporal resolution [41] and the site meteorological measurements data gathered from [42] with hourly temporal resolution. The future meteorological data of the year 2050, considering RCP 8.5, relies on dynamical downscaling, following the approach outlined by the IEA EBC Annex 80 [43]—Weather Data Task Force. The most advanced approaches and tools for producing future global projections and weather files are referenced [44].

2.2. Remote Sensing Technique to Retrieve SUHI

In recent years, due to an increasing number of extreme meteorological events potentially related to climate change, growing attention has been paid to the operational use of satellite remote sensing applied to emergency management applications. This increased focus can be attributed to the substantial and prompt availability of diverse remotely sensed data types, along with geospatial information collected in situ [45]. In this study, we employed remotely sensed data and techniques to detect the SUHI effect and select our study case.

In the initial phase of the study, the methodologies employed for the SUHI computational mapping process were delineated into seven discrete steps.

2.2.1. Top of Atmospheric Spectral Radiance

As demonstrated in Figure 2, the initial step entails the calculation of the Top of Atmospheric (TOA) $L(\lambda)$ spectral radiance utilizing Equation (1) [46,47] with the Raster Calculator Tool incorporated within ArcGIS Pro 3.4.

$$\text{TOA}(L(\lambda)) = \text{ML} \times \text{Qcal} + \text{AL}. \quad (1)$$

TOA ($L(\lambda)$) stands for Total Spectral Radiance ($\text{Watts}/(\text{m}^2 * \text{srad} * \mu\text{m})$), ML stands for the band-specific Multiplicative Rescaling Factor, Qcal refers to Band 10 of Landsat 9, and AL stands for the Band-Specific Additive Rescaling Factor. The MTL file is the only way to obtain the values for ML, Qcal, and AL. AL can be found in the MTL file by searching for RADIANCE ADD BAND 10 = 0.10000, and ML can be found in the MTL file by searching for RADIANCE MULT BAND 10 = 3.8×10^{-4} . Finally, Qcal is obtained by selecting Band 10 of the Landsat 9 image.

2.2.2. The Conversion of Radiance to At-Sensor Temperature

Subsequent to determining the TOA, the subsequent step entails the conversion of spectral radiance to the Top of the Atmosphere Brightness Temperature (BT), as delineated in Equation (2) [46,47]. This conversion is performed by utilizing the thermal constants K1 and K2, which are obtained from the MTL file document, and the Total Spectral Radiance ($L\lambda$), which is the result of the preceding step.

$$\text{BT} = \frac{\text{K2}}{\ln\left[\left(\frac{\text{K1}}{L\lambda}\right) + 1\right]} - 273.15. \quad (2)$$

It can be demonstrated that K1 and K2 can be discovered by finding the values of CONSTANT BAND 10, which are 799.0284 and 1329.2405, respectively.

2.2.3. The Normalized Different Vegetation Index (NDVI) Method for Emissivity Correction

The subsequent stage in the procedure entails the employment of the NDVI method for emissivity correction, as delineated in Equation (3) [46,47]. This method holds paramount importance, as it is instrumental in determining the proportion of vegetation (P_v) through its application in calculating the Land Surface Emissivity (ϵ), a variable that is inextricably linked to the P_v [46,47].

$$\text{NDVI} = \frac{\text{NIR}(\text{band } 5) - \text{Red}(\text{band } 4)}{\text{NIR}(\text{band } 5) + \text{Red}(\text{band } 4)}. \quad (3)$$

2.2.4. Calculation of the Proportion of Vegetation

Substituting the results of Equation (3) into Equation (4) [46,47] yields the proportion of vegetation (P_v).

$$P_v = \left(\frac{\text{NDVI} - \text{NDVI}_{\min}}{\text{NDVI}_{\max} - \text{NDVI}_{\min}} \right)^2. \quad (4)$$

2.2.5. Calculation of Land Surface Emissivity

Afterwards, the next step is to calculate the (ϵ) using Equation (5) [46] with the value of 0.004 and the correction value of 0.986 from the MTL file.

$$\epsilon = 0.004 \times P_v + 0.986. \quad (5)$$

2.2.6. Retrieving the Land Surface Temperature

The final step prior to calculating the SUHI value was to compute the Land Surface Temperature (LST). Utilizing the BT value previously obtained from Equation (2), the LST in degrees Celsius ($^{\circ}\text{C}$) can be calculated through the application of Equations (6) and (7) [46,47] and the input parameters delineated in Table 3.

$$\text{LST} = \frac{\text{BT}}{\left\{ 1 + \left[\left(\frac{\lambda \text{BT}}{\rho} \right) \ln \epsilon \right] \right\}}. \quad (6)$$

$$\rho = h \frac{c}{\sigma} = 1.438 \times 10^{-2} (\text{mK}). \quad (7)$$

Table 3. Parameters for land surface temperature calculation.

Parameters	Values
Emitted radiance (λ)	10.800 (nm)
Stefan–Boltzmann constant (σ)	5.667×10^{-8} ($\text{W}/\text{m}^2\text{k}^4$)
Light velocity (c)	2.998×10^4 (m/s)
Planck constant (h)	6.626×10^{-34} (J)

2.2.7. Estimation of SUHI

The term SUHI has been frequently employed to denote the difference in surface temperature between urban and rural areas. This can also be defined by quantification to consider urban surfaces' local and regional climate change. The SUHI is calculated using the following Equation (8) [48], where T is LST, T_m is LST mean, and T_{sd} is the standard deviation of LST.

$$\text{SUHI} = \frac{T - T_m}{T_{sd}}. \quad (8)$$

2.3. Numerical Simulation to Retrieve Canopy Urban Heat Island Considering Urban Geometry Modeling and the Simulation Period

Accurate building footprints have significant implications for urban planning and infrastructure management [49]. The geometric model that served as the foundation for all simulations was developed using the Rhinoceros 8 modeler. The dragonfly model was created based on dragonfly buildings from footprint geometry (horizontal Rhino surfaces). The buildings were created with the extrusion from building footprints based on digital elevation models, which represent an approximation of the building massing [50]. In addition to the selection of the urban site, the decision was made to decrease the run time for the comfort analysis by employing short time periods of four days taken from typical weeks in the (stat) file in the weather file of the weather station in Turin-Caselle Airport [41]

(Table 4). The time period from 8:00 to 18:00, when the majority of activities are conducted, was selected for the simulation [12,33,51,52].

Table 4. Simulation time periods.

Typical Weeks	Selected Data
Extreme Cold Week (13 January–19 January)	12 January
Typical Spring Week (29 March–4 April)	29 March
Extreme Hot Week (27 July–2 August)	29 July
Typical Autumn Week (13 October–19 October)	15 October

2.3.1. Urban Heat Island Modeling with the Urban Weather Generator

UHI was incorporated into the present study by morphing the TMY weather data of the weather station through the integration of the validated Urban Weather Generator (UWG). The UWG approximates the thermal conditions of a city and utilizes several key geometric and material variables, as outlined in Table 5. These parameters are then entered into a generic model of the urban canyon, after which energy balance calculations are performed. Ultimately, the UWG morphed a TMY file, thereby adjusting the air temperature and relative humidity to reflect the urban conditions. Additionally, it incorporated anthropogenic heat fluxes resulting from exfiltration and waste heat from building HVAC systems [53–55].

Table 5. Ladybug urban weather generator simulation settings.

Model Parameters and Buildings Construction Set	
Climate Zone	Koppen Classification [3]/Cfa
Building Vintage	Pre-1980
Construction Type	Mass
Program	Medium Office [50], Conditioned
Terrain Properties	
Albedo (Reflectivity)	0.25 [56]
Thickness	0.5 (m)
Conductivity (Typical of Asphalt)	1 (W/mK)
Volumetric Heat Capacity (Typical of Asphalt)	1.6E6 (J/m ³ K)
Traffic Parameters	
Maximum Sensible Anthropogenic Heat	20 (W/m ²)
Albedo	0.25 [57]
Fraction of the Absorbed Solar Energy by Trees	0.7
Fraction of the Absorbed Solar Energy by Grass	0.5
EPW Site Parameters	
Obstacles Height	0.01 (m)
Vegetation Coverage	0.9
Temperature Height	17
Wind Height	10
Boundary Layer Parameters	
Day Height	1000 (m)
Night Height	80 (m)
Inversion Height	150 (m)
Circulation Coefficient	1.2
Exchange Coefficient	0.2 [54]
Model Geometric Variables	
Average Height	15.7 (m)
Footprint Density	0.41
Facade to Site	1.4

Table 5. Cont.

Green Façade Characteristics	
Air Gap	0.05 (m) [27]
Plant Height	0.1 (m)
Leaf Area Index (LAI)	3 [27]
Substrate	0.05 (m)
Leaf Reflection	0.22
Leaf Emission	0.95
Soil Reflection	0.3
Soil Emission	0.9
Stomata Resistance	180 (s/m)
Soil Thickness	0.22 (m)
Soil Conductivity	0.35 (W/mK)
Soil Density	1100 (kg/m ³)
Soil-Specific Heat	1200 (J/kg K)

2.3.2. Mean Radiant Temperature Calculation

In this section of the research, the objective is to evaluate the impact of a canyon's geometry and surface characteristics, including ground and facade reflectivity and emissivity, on the Tmrt simulation and its spatial distribution. This analysis is conducted using the method outlined in the literature [52,53,56].

In the first step of calculating, base longwave radiation would be computed Equation (9) [53,56].

$$\text{LWMRT} = \left[\sum_{i=1}^N F_i T_i^4 \right]^{1/4} - 273.15 \text{ } ^\circ\text{C}. \quad (9)$$

We consider T_i to be equivalent to the surface temperature, as derived from the EnergyPlus simulation. F_i is defined as the view factor for each surface, calculated through the ray-tracing capabilities of the Rhino 3D modeling engine. The model also incorporates the sky temperature and longwave loss to the sky in Equation (10) [53,56], utilizing the horizontal infrared radiation contained within the TMY data.

$$T_{\text{sky}} = \frac{L_a}{(\epsilon_{\text{person}} \sigma)^{1/4}}. \quad (10)$$

In the context of outdoor shortwave solar radiation, which is defined as the direct incidence of solar radiation upon individuals, the SolarCal model [58] of ASHRAE-55 is defined. The SolarCal model is based on the Effective Radiant Field (ERF), a metric of the net radiant energy flux to or from the human body, as defined by Equation (11) [53,56]. ERF is employed to delineate the supplementary (positive or negative) long-wave radiation energy at the body surface when the surrounding surface temperatures deviate from the air temperature. It is in (W/m²), where area refers to body surface area.

$$\text{ERF}_{\text{solar}} = (0.5 \cdot f_{\text{eff}} \cdot f_{\text{svv}} \cdot (I_{\text{diff}} \cdot I_{\text{th}} \cdot R_{\text{floor}}) + A_p \cdot f_{\text{bes}} \cdot I_{\text{dir}} \cdot AD) \cdot (a_{\text{sw}} \cdot a_{\text{lw}}). \quad (11)$$

This ERF is converted into a Tmrt delta using the following Equation (12) [53,56]:

$$\text{ERF} = f_{\text{eff}} h_r (\text{MRT} - \text{LWMRT}). \quad (12)$$

2.3.3. Mean Radiant Temperature Validation

In order to statistically evaluate the acceptability of the simulation and output for measuring Tmrt, a comparison will be made between them and the site-measured sensor data with the characteristics provided in Table A1. The validation was analyzed using the Mean

Bias Error (MBE) Equation (13) and the Cumulative Variation of Root Mean Squared Error (CVRMSE) Equations (14) and (15), in accordance with the ASHRAE Guideline 14 [52,59].

$$MBE = \frac{\sum_{i=1}^{N_p} (M_i - S_i)}{\sum_{i=1}^{N_p} M_i} \tag{13}$$

$$CVRMSE = \frac{\sqrt{\sum_{i=1}^{N_p} (M_i - S_i)^2 / N_p}}{M_p} \tag{14}$$

$$\left(\overline{M_p} = \frac{\sum_{i=1}^{N_p} M_i}{N_p} \right) \tag{15}$$

According to the ASHRAE Guideline 14, the acceptable limits for calibration are delineated as follows. When analyzing hourly data, the results must be within ±10% MBE and ≤30% CVRMSE. The Tmrt and validation results for the MBE and the CVRMSE, respectively, are provided in Table 6 and Figure 3.

Table 6. Mean radiant temperature validation. MBE: Mean Bias Error, CVRMSE: Cumulative Variation of Root Mean Squared Error.

Date	MBE	CVRMSE
12 January	−8.96%	22.12%
29 March	−8.35%	17.56%
15 October	−1.97%	20.15%
29 July	5.22%	14.98%



Figure 3. Mean radiant temperature validation.

2.3.4. Measuring Outdoor Thermal Comfort (UTCI)

UTCI, as an international standard for outdoor temperature sensation, is a thermal comfort model that quantifies how people perceive given weather conditions based on the range and stress category (Table 7) and is one of the most common temperatures used by meteorologists. While UTCI is designed to be valid in all climates and seasons, it operates under the assumption that human subjects are walking and that they naturally adapt their clothing to the outdoor temperature. For outdoor situations that do not fit these criteria, the Physiological Equivalent Temperature (PET) model is recommended. The calculation of the average UTCI over the specified time series, ranging from 8:00 to 18:00, necessitates the establishment of input parameters. These parameters, which are instrumental in determining the outdoor comfort levels, encompass wind speed data extracted from the designated weather file, mean air temperature measurements, relative humidity levels derived from the urban weather generator, and surface temperature values obtained from the URBANopt simulation conducted using EnergyPlus [60].

Table 7. UTCI stress categories and ranges.

Stress Category	Range °C
Extreme Cold Stress	UTCI < −40
Very Strong Cold Stress	−40 ≤ UTCI < −27
Strong Cold Stress	−27 ≤ UTCI < −13
Moderate Cold Stress	−12 ≤ UTCI < 0
Slight Cold Stress	0 ≤ UTCI < 9
No Thermal Stress	9 ≤ UTCI < 26
Slight Heat Stress	26 ≤ UTCI < 28
Moderate Heat Stress	28 ≤ UTCI < 32
Strong Heat Stress	32 ≤ UTCI < 38
Very Strong Heat Stress	38 ≤ UTCI < 46
Extreme Heat Stress	46 < UTCI

2.3.5. Modeling of Green Wall

As stated in the article [61], which provides a categorization and comparison of various vertical greenery systems, including Green Barrier Systems, Green Coating Systems, and GWs, green walls have been found to be more effective in reducing outdoor surface temperatures and operative temperature. In this case, three categories have been proposed: the Mur Vegetal (MV), the Light Systems (LS), and the Heavy Systems (HS). The distinction between HS and LS lies in the soil thickness (less or greater than 15 cm, respectively). In the present study, LS with the material properties delineated in Table 5 was employed. The GWs systems exhibit remarkable capacity to reduce the surface temperatures, which are also lower than those of the ambient air. Among the various systems, LS and HS have emerged as the most efficient ones in reducing the maximum temperature. However, the HS has a greater reduction in operative temperature in summer, while MV's effect on operative temperature in winter is greater. The thickness of the air gap and the type of soil are almost irrelevant in influencing the external surface temperatures, while the variation in LAI influences the external surface temperatures. Green walls (GWs) are characterized by the necessity of a higher degree of greater technical specialization in comparison to the other categories. The technology package (which includes the plants and the substrate) is supported by a subsystem and forms a gap with the walls, thereby exhibiting the characteristics of a ventilated façade. The ventilated cavity has been modeled as a separate thermal zone, and it has been conceptualized as a leaky building with a flow per exchange area of 0.0006 (m³/s per m² facade) and air changes per hour (ACH) of 3 [62,63].

2.4. Evaluating Carbon Emission Intensity in Energy System

The calculation can be utilized in the design of low- and net-zero-carbon buildings and districts. Carbon dioxide (CO₂) emissions per total energy supply refer to the quantity of kilograms of CO₂ released to produce a megawatt-hour (MWh) of energy. In this study, input emissions per total energy supply will be employed to calculate carbon intensity for both electricity and heating/cooling systems. The most recent carbon emissions of the Italian total energy supply for the year 2019 [64] were utilized as the reference value to compute the changes in energy consumption of our model and, consequently, the cei for the future projection 2050 emission report. In this study, the heating and cooling HVAC system was defined as a window AC with a baseboard gas boiler, and the service hot water system was defined as an electric water heater. The aggregated emission per total energy supply for the year 2019, with a value of 178.5 (kgCO₂/MWh), was considered in our analysis.

3. Results

3.1. SUHI Detection and Site Selection

An analysis of surface temperature distribution across the Piedmont region of Italy revealed a significant thermal gradient, with temperatures ranging from 54 °C to 91 °C (Figure 4a). Statistical analysis indicated that nearly the entirety of the city would experience SUHI. Via della Consolata exhibited a very-high-intensity heat island region, which was selected as the study area. The Santuario della Consolata (7°40.7473753' E 45°4.6011994' N) is located at the center of this area (Figure 4b). The meteorological sensors mounted on the building record the following parameters: dry bulb temperature (°C), wind speed (m/s) and direction, relative humidity (%), atmospheric pressure, and irradiances (W/m²).

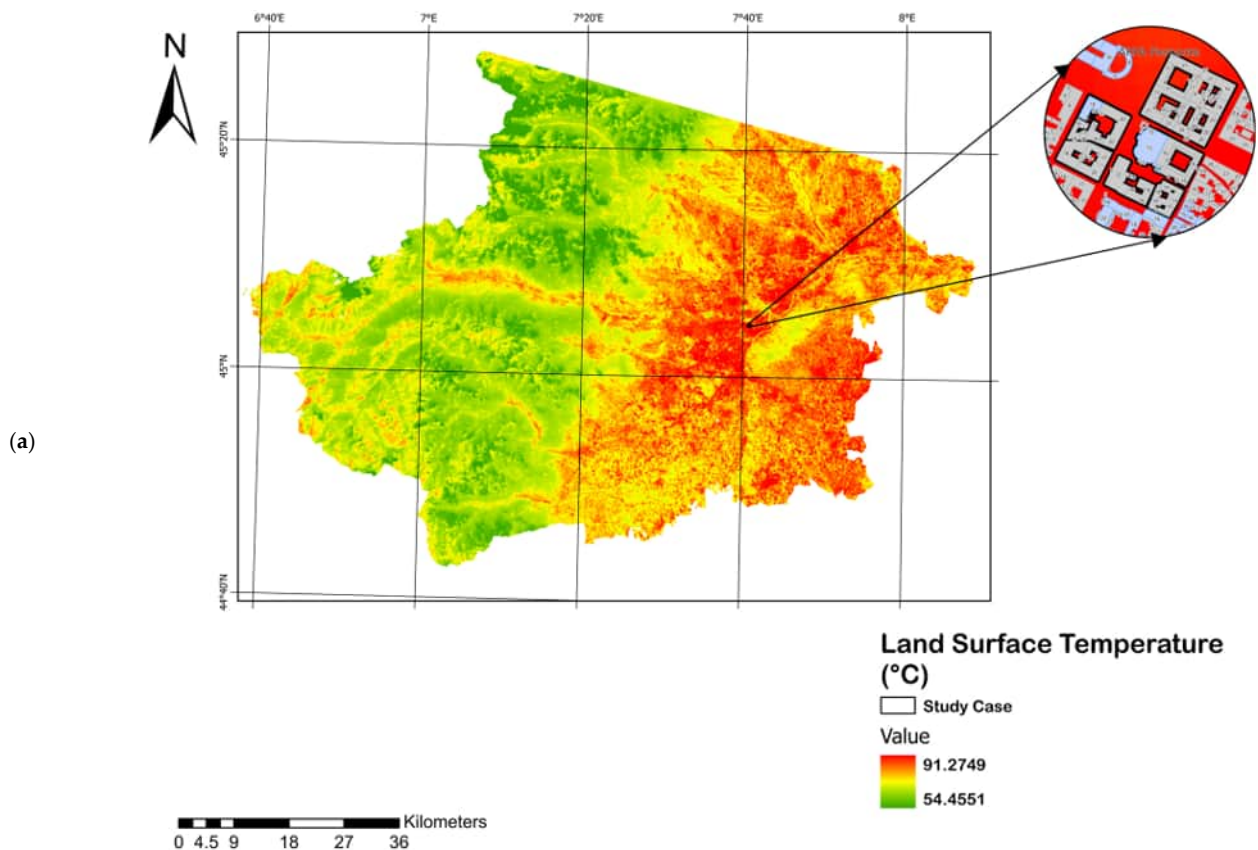


Figure 4. Cont.

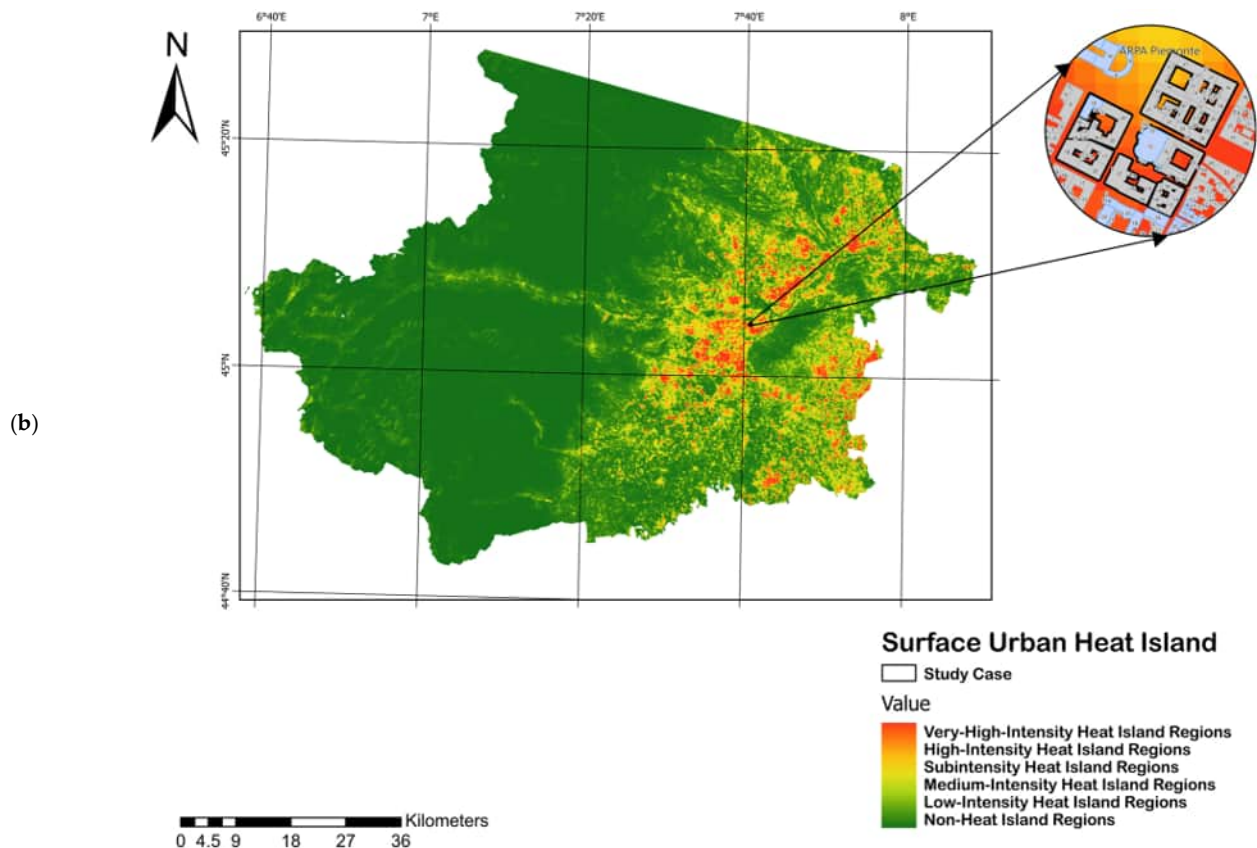


Figure 4. (a) Land surface temperature ($^{\circ}\text{C}$) and study area detection; (b) SUHI ranges and study area detection.

3.2. Impact of Green Walls on Outdoor Air Temperature for Current Condition and Future Projection

The installation of green walls exhibited intricate temporal variations in outdoor air temperature (Table 8). Under the prevailing climate conditions, the most substantial effects were observed during winter and spring, where temperature fluctuations ranged from a decrease of $0.3\text{ }^{\circ}\text{C}$ to an increase of $1.3\text{ }^{\circ}\text{C}$ on 12 January and from a reduction of $1.3\text{ }^{\circ}\text{C}$ to an increase of $1.2\text{ }^{\circ}\text{C}$ on 29 March. These variations exhibited robust diurnal and seasonal patterns, with the most pronounced cooling effects typically occurring until mid-afternoon hours, a phenomenon that persisted until 15 October. In contrast, summer conditions, as evidenced by measurements collected on 29 July, exhibited more modest and uniform modifications, ranging from $0\text{ }^{\circ}\text{C}$ to $+0.4\text{ }^{\circ}\text{C}$.

In considering the broader context of urban heat island effects, future climate projections for 2050 are anticipated to exacerbate this phenomenon (Figure 5). However, the implementation of green walls could help counteract this trend by producing smaller temperature increases and more significant reductions, ranging from $-1.6\text{ }^{\circ}\text{C}$ to $0.7\text{ }^{\circ}\text{C}$, which highlight their potential as an effective mitigation strategy in the face of climate change. For instance, on 29 July, air temperatures under the current climate scenario exhibited some increases throughout the day. In contrast, future climate projections for 2050 demonstrated a consistent decline in temperature during the mid-afternoon hours. A similar trend was observed in winter. While early mornings—8:00 AM and 9:00 AM—under current conditions exhibited slight increases in air temperature, future projections indicated a notable decrease throughout the day, with more substantial reductions. The enhanced effectiveness under future climate scenarios suggests that green walls may become increasingly valuable as a climate adaptation strategy.

Table 8. Air temperature variation ($^{\circ}\text{C}$) after introducing a green wall for all the simulation periods under current and future projection climate conditions.

Current Weather Condition											
Date	Hour										
	8:00	9:00	10:00	11:00	12:00	13:00	14:00	15:00	16:00	17:00	18:00
12 January	0.6	1.3	−0.2	−0.2	−0.2	−0.2	−0.3	−0.2	−0.3	−0.2	0.6
29 March	1.1	0.1	0	0	0	−0.1	−0.1	0	1.2	0.3	−1.3
29 July	0.2	0	0	0	0	0	0	0	0	0	0.4
15 October	0	0	0	0.1	0	0	−0.1	0	−0.4	−0.6	−0.6
Future Projection 2050 (RCP8.5)											
Date	Hour										
	8:00	9:00	10:00	11:00	12:00	13:00	14:00	15:00	16:00	17:00	18:00
12 January	−0.3	−0.3	−0.3	−1.6	−0.3	−0.3	−0.2	−0.3	−0.3	−0.4	0.1
29 March	−0.2	−0.1	0	0	0	−0.1	0.3	0.2	0.3	0.7	0.5
29 July	0	0	0	0	0	0	0	−0.1	−0.1	−0.1	0.2
15 October	0	0.1	0	0	0	0	0	0	−0.1	−0.1	−0.1

**Figure 5.** Comparison of air temperature ($^{\circ}\text{C}$) during current and future projection (2050) climate conditions.

3.3. The Enhancement Effect of the Green Wall on Mean Radiant Temperature and Outdoor Comfort Under Current and Future Climate Projections (2050)

An analysis of the cooling effect of the green wall on average T_{mrt} under current conditions and future climate projections is presented in Figures 6 and 7. Under current climate conditions, the green wall showed varying effects across different seasons. On 12 January, the results show an insignificant reducing effect with the values from -0.41°C to -0.22°C , showing a relatively modest effect with colder outdoor conditions, lower sun angle, and lower evapotranspiration efficiency. On 29 March the range of reductions was relatively higher, with the range from -0.64°C to -0.34°C . In contrast, on 29 July, the

green wall exhibited the most substantial impact with the reduction, ranging from $-1.10\text{ }^{\circ}\text{C}$ to $-0.59\text{ }^{\circ}\text{C}$, which is the consequence of having higher outdoor temperatures typical of summer, showing the effectiveness of the green wall in mitigating the UHI effect. Finally, cooler air temperatures on 15th October showed a smaller decrease in Tmrt from $-1.07\text{ }^{\circ}\text{C}$ to $-0.57\text{ }^{\circ}\text{C}$.

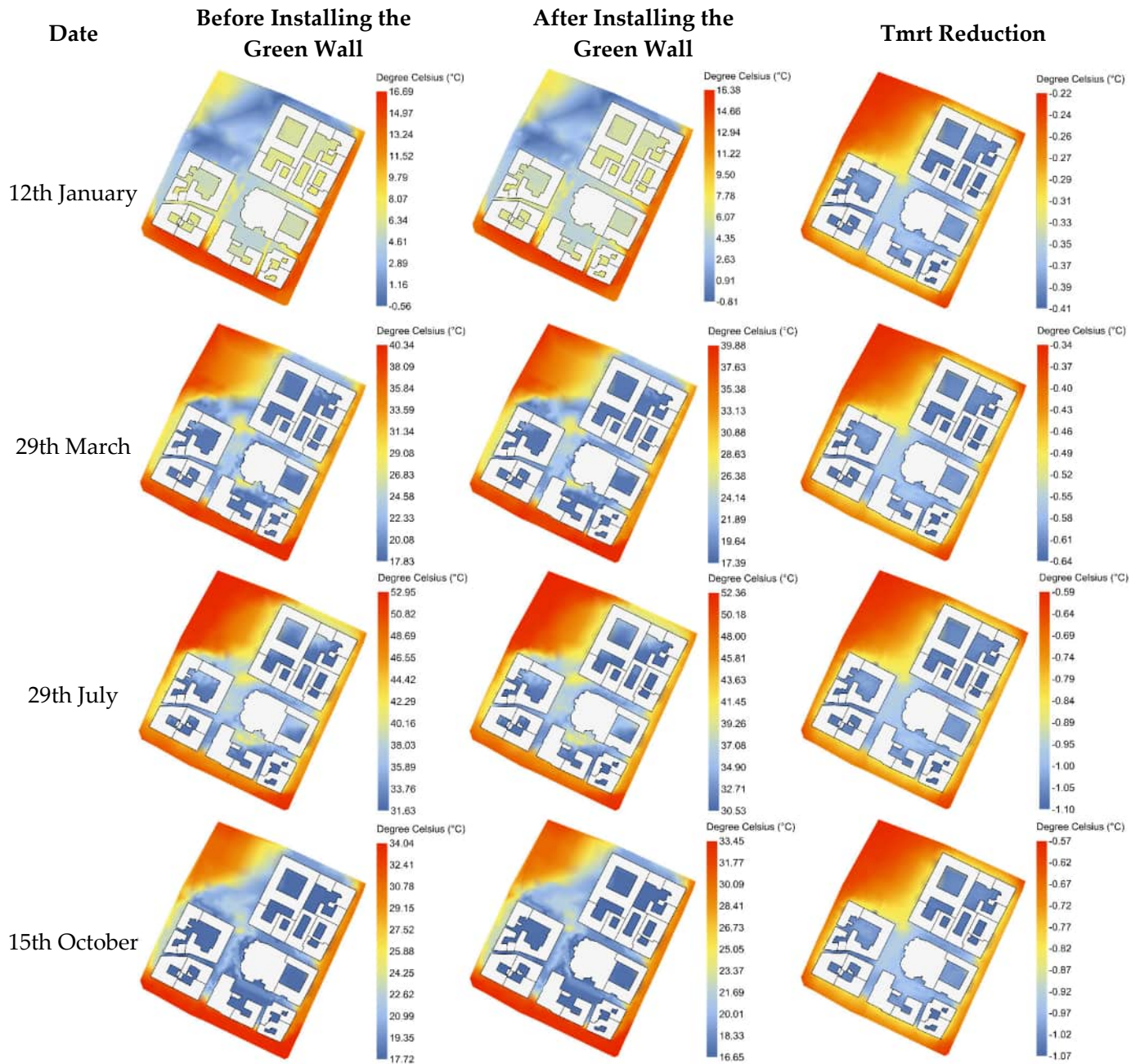


Figure 6. Mean radiant temperature (Tmrt) $^{\circ}\text{C}$ spatial heat map before and after the installation of the green walls and the enhancement effect of green walls under current weather conditions.

In the case of the future projection 2050, in all the simulation periods we will experience higher outdoor air temperatures (Figure 5). In autumn and winter, instead of having warmer outdoor temperatures, the cooling effect of green walls was less impactful, with the mitigating from $-0.34\text{ }^{\circ}\text{C}$ to $-0.18\text{ }^{\circ}\text{C}$ on 15 October and $-0.13\text{ }^{\circ}\text{C}$ to $-0.07\text{ }^{\circ}\text{C}$ on 12 January. Considering having lower spatial Tmrt in 2050 because of lower radiation (Figure A1), and since solar radiation is a key driver of evapotranspiration, this condition

results in less energy available to evaporate water from the soil and transpire water through the plants, thus having less cooling potential of green walls. Similarly, on 29th March, by considering having relatively higher air temperature and lower solar radiation (Figure A1), leading to lower spatial Tmrt, and better cooling performance with the averaged reduction from $-1.25\text{ }^{\circ}\text{C}$ to $-0.67\text{ }^{\circ}\text{C}$. This could be the result of a greater temperature difference between air and surfaces resulting in better heat transfers.

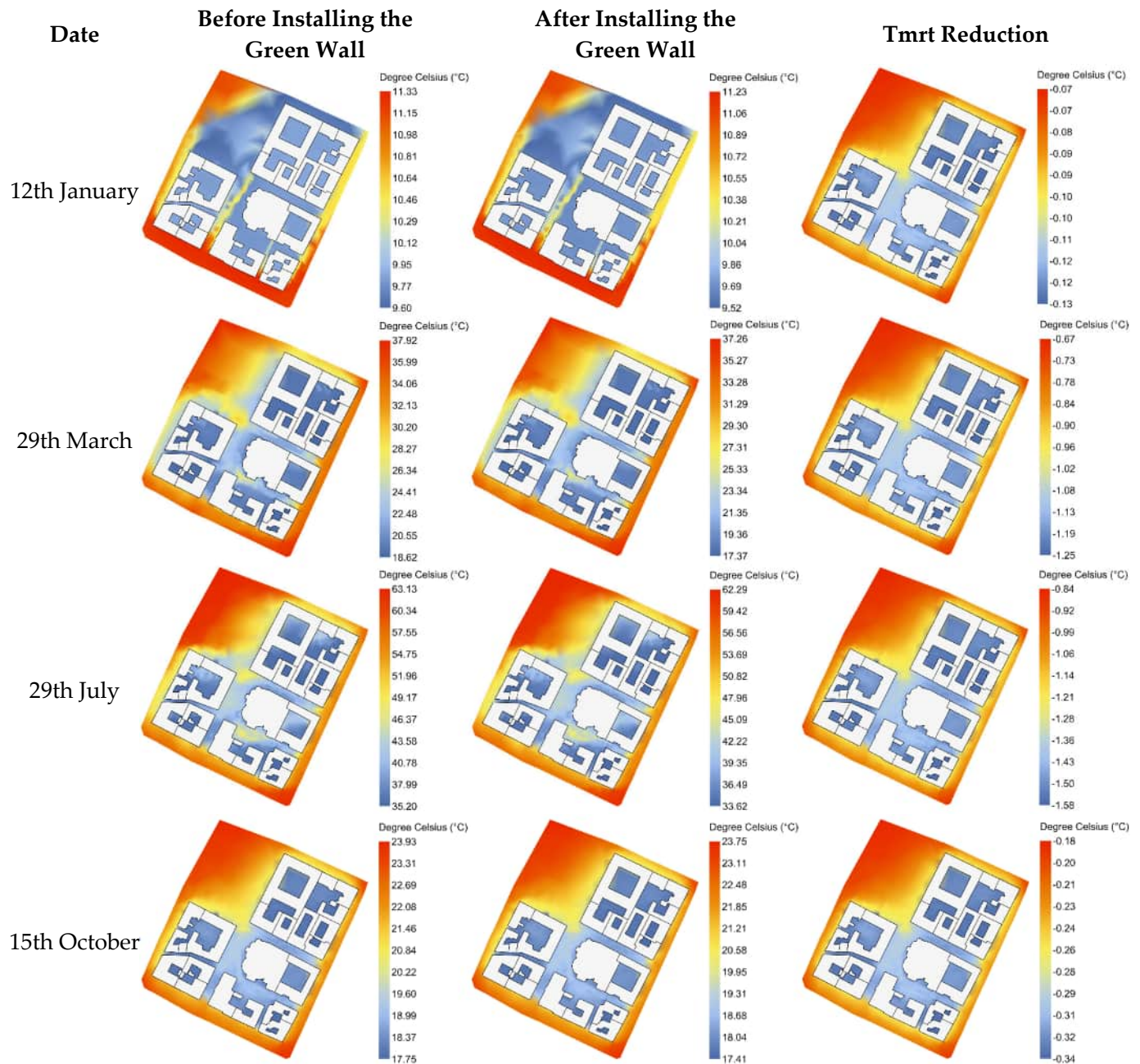


Figure 7. Mean radiant temperature (Tmrt) $^{\circ}\text{C}$ spatial heat map before and after the installation of the green walls and the enhancement effect of the green walls for future projection (2050) weather conditions.

On 29 July 2050, the relatively higher air temperature and solar radiation compared to current weather conditions cause an increase in average Tmrt and evapotranspiration by the leaves. In this case, the higher rate of evapotranspiration would result in better cooling performance of green walls with values from $-1.58\text{ }^{\circ}\text{C}$ to $-0.84\text{ }^{\circ}\text{C}$. It is also worth noting that in all cases, the greatest reduction in Tmrt occurred in the canyons and courtyards

with lower SVF and less direct sunlight exposure (Figure 8). In these areas, the main cause of higher T_{mrt} is longwave radiation emitted from walls and pavements as they accumulate heat during the day and re-radiate it to the surrounding area, thus the heat has restricted the scattering paths. The shading effect of green walls would reduce the surface temperatures, hence decreasing longwave radiation emissions. Compared to open areas with better heat dissipation, this leads to a more pronounced cooling effect in low-SVF areas, where longwave radiation plays a dominant role. Additionally, in open areas, the T_{mrt} would decrease more in areas closer to the walls.

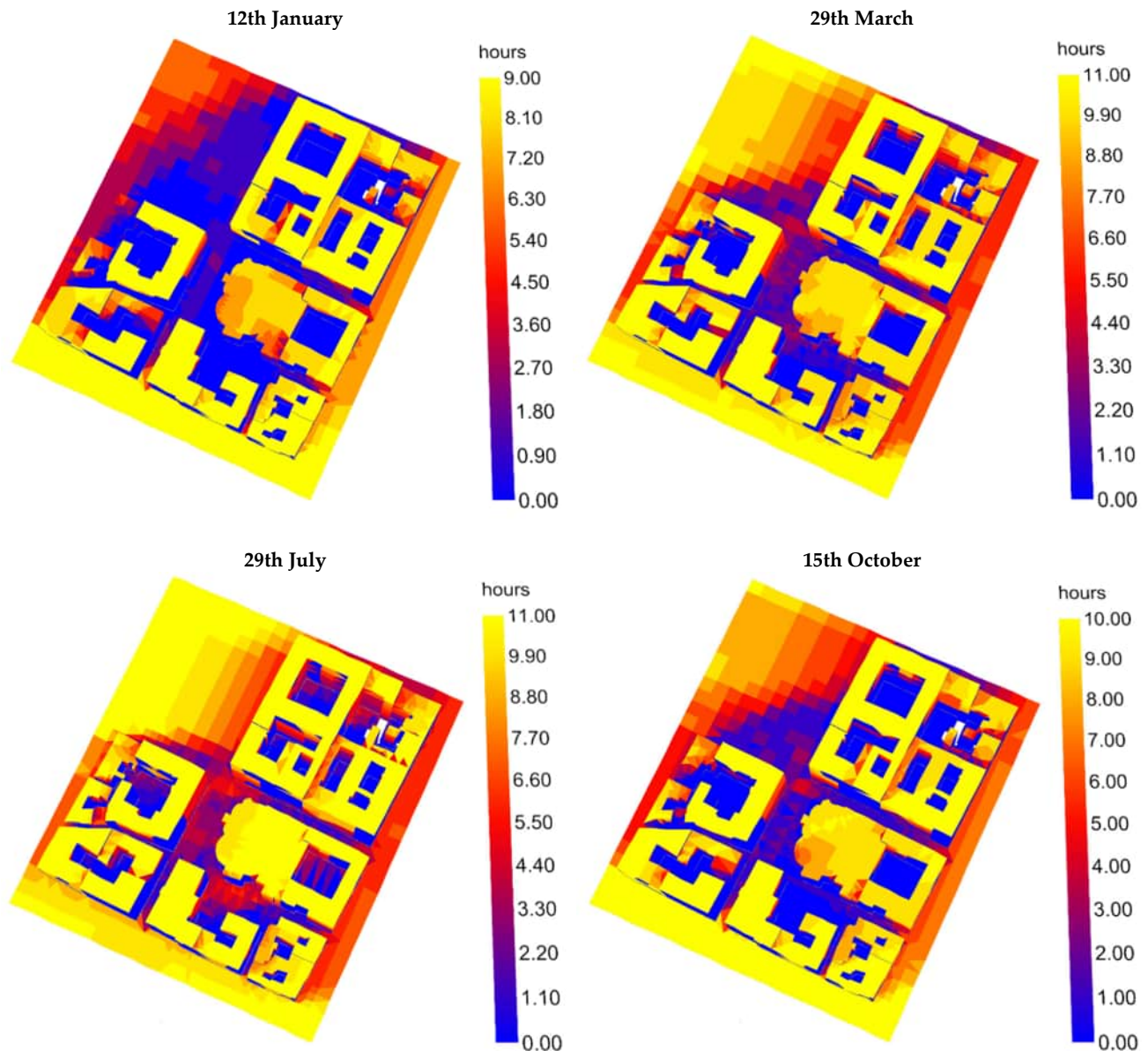


Figure 8. Number of hours of direct sunlight received in each simulation period.

As presented in the literature, the most influential parameters affecting UTCI are T_{mrt} [16], air temperature, and relative humidity. It can be shown in Figures 9 and 10 that the average UTCI experienced a reduction in all simulation periods after introducing the green wall to the model. The maximum reduction was recorded on 15 October by 0.44 °C and the minimum reduction on 12 January by 0.12 °C, under the current weather conditions.

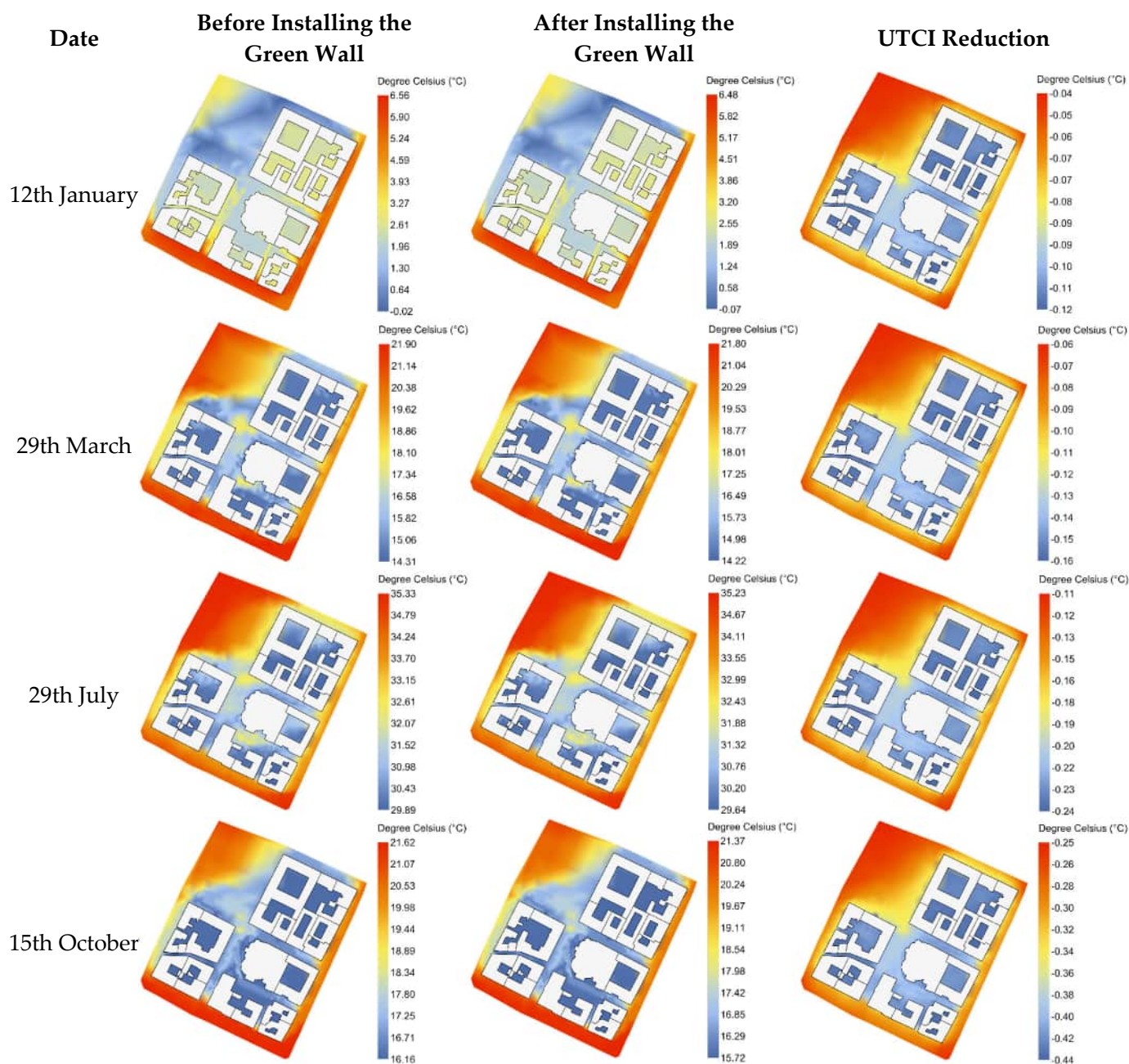


Figure 9. Outdoor comfort (UTCI) spatial heat map before and after the installation of the green walls and the enhancement effect of the green walls under current weather conditions.

Comparing the changes in outdoor comfort between future projection 2050 and current weather conditions, on 12 January and 29 July, we will experience worsening in outdoor comfort, which is the consequence of the greatest increase in air temperature (Figure 5). However, the enhancement effect of the green wall on thermal comfort would be maximum on 29 July by 0.40 °C.

In contrast, the change in air temperature was not significant on 29 March and 15 October. Furthermore, we will experience better outdoor comfort on 15 October with the least decreasing effect of the green wall and on 29 March, which corresponds to the lower T_{mrt} predicted in 2050.

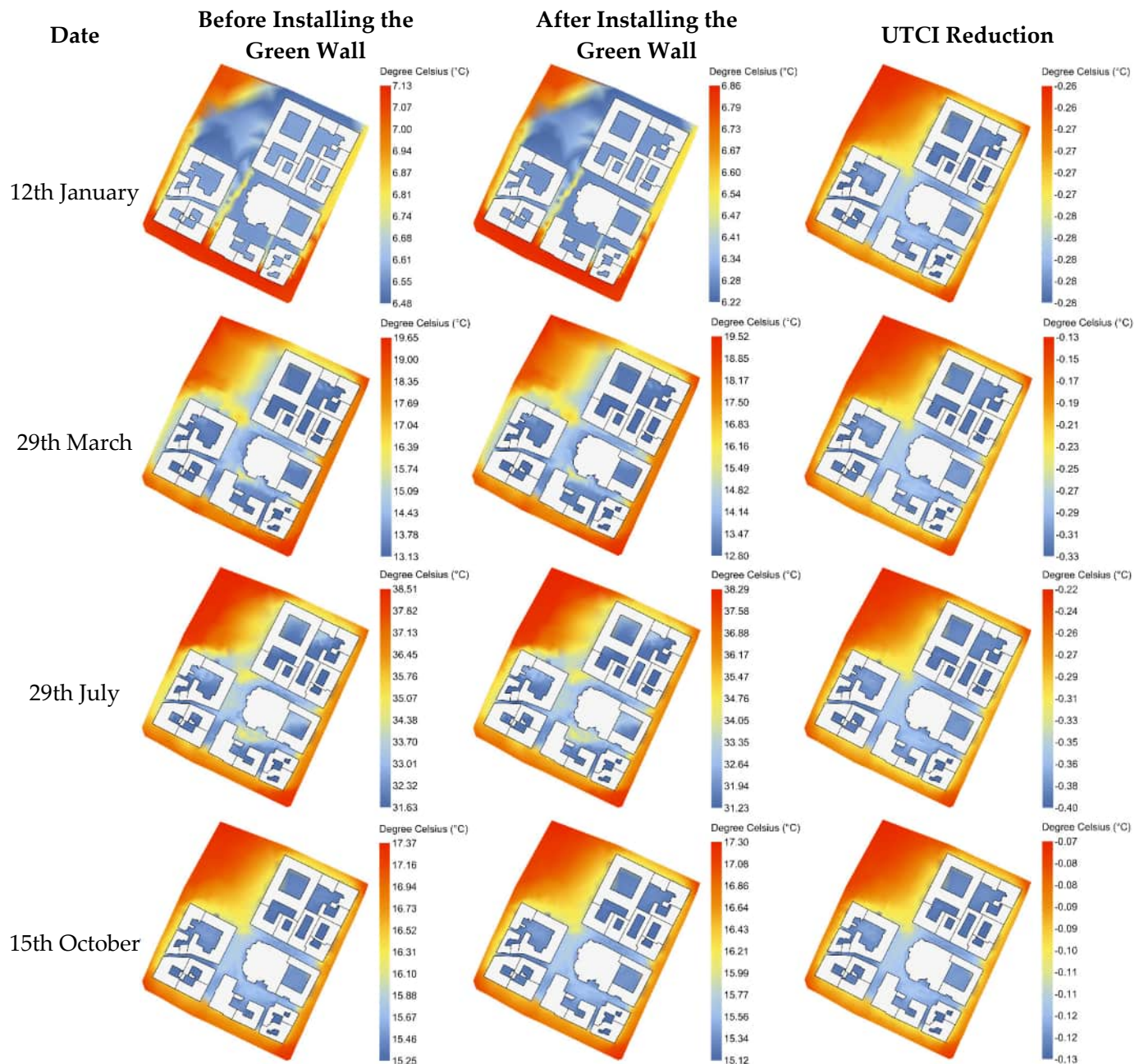


Figure 10. Outdoor comfort (UTCI) spatial heat map before and after the installation of the green walls and the enhancement effect of the green walls for future projection (2050) weather conditions.

3.4. Mitigation Effect of Green Walls in the Condition of Maximum Direct Normal Radiation

During the simulation period of the hottest week, climate change would amplify the T_{mrt} and UTCI. This is due to an increase in air temperature on 29th July at noon by 4.5 °C and maximum solar radiation with the values of 634 (Wh/m^2) and 749 (Wh/m^2) in current and future weather conditions, respectively. However, the cooling effect of the green wall will be more pronounced in 2050. The maximum reduction in T_{mrt} was recorded at 1.92 °C and 2.27 °C, and the maximum enhancement in outdoor comfort was recorded at 0.51 °C and 0.55 °C under current and future climate projections, respectively (Figure 11).

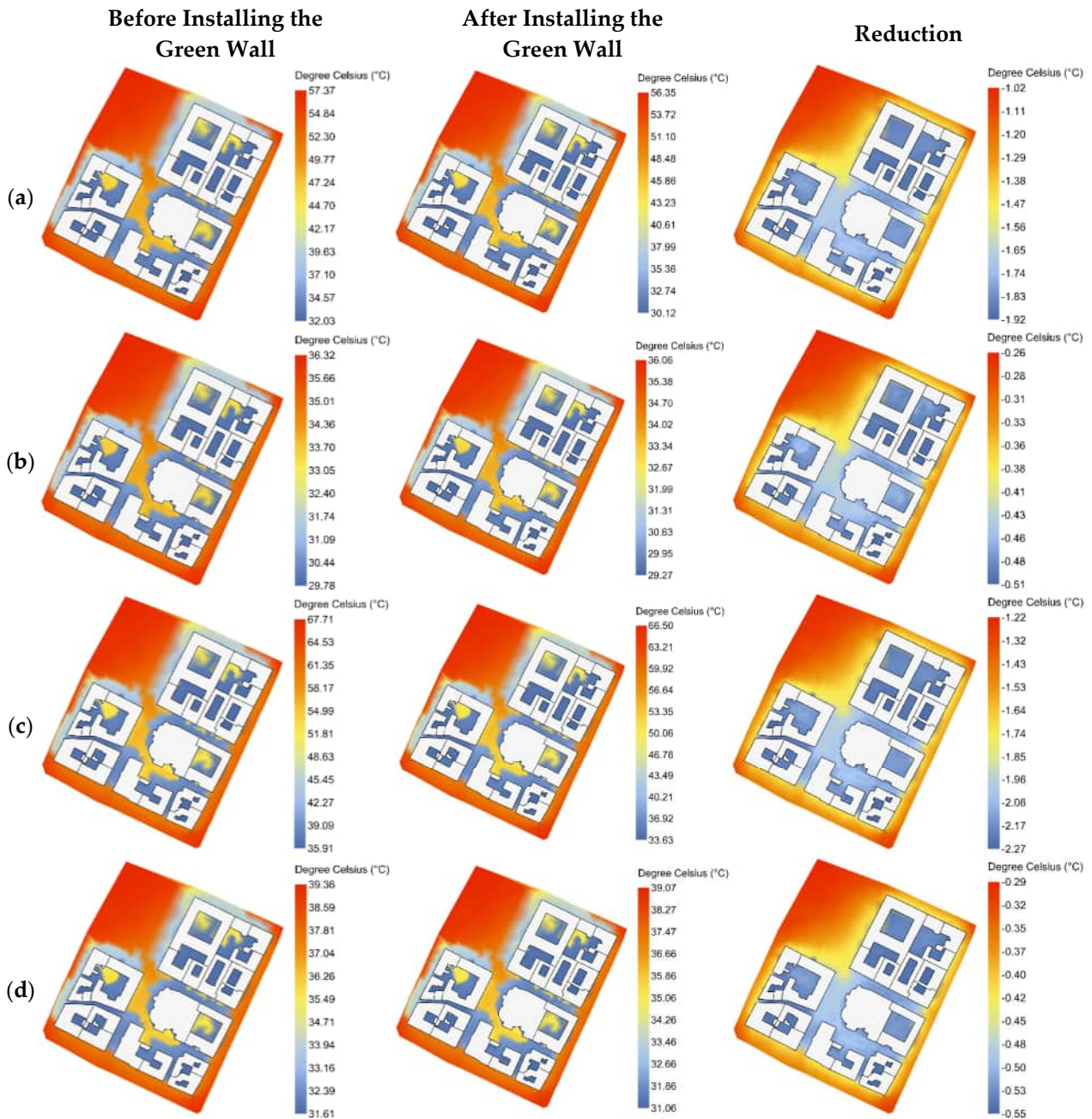


Figure 11. Enhancement of mean radiant temperature (T_{mrt}) °C and outdoor comfort (UTCI) at 12:00 PM on 29 July when the direct solar radiation is maximum; (a) mean radiant temperature changes under current climate conditions; (b) outdoor comfort changes under current climate conditions; (c) mean radiant temperature changes under future projection (2050) climate conditions; (d) outdoor comfort changes under future projection (2050) climate conditions.

3.5. Impact of Green Walls on Carbon Emission Intensity in 2050

On 12 January, there was an overall increase of 0.022 (kg CO₂/m²) in the (cei), primarily due to an increase in the heating demand from 0.495 (kg CO₂/m²) to 0.518 (kg CO₂/m²). Conversely, on 15th October, the total increase in (cei) amounted to 0.01 (kg CO₂/m²), with an increase in heating demand from 0.012 (kg CO₂/m²) to 0.022 (kg CO₂/m²). Conversely, on 29 July, a maximum reduction of 0.031 (kg CO₂/m²) was observed. This decline is attributed to a reduction in cooling demand from 0.085 (kg CO₂/m²) to 0.054 (kg CO₂/m²). The implementation of the green walls on 29 March led to a decline in overall cooling demand of 0.026 (kg CO₂/m²), reducing it from 0.028 (kg CO₂/m²) to 0.002 (kg CO₂/m²).

Concurrently, there was an increase of 0.016 (kg CO₂/m²) from 0.025 (kg CO₂/m²) to 0.041 (kg CO₂/m²) in heating demand.

As demonstrated in Table 9, the carbon emission results for each simulation day are based on the total gross floor area of 21,741 (m²). The installation of the green walls has been shown to result in a cooling effect, which would lead to an overall increase in energy demand during colder months and a reduction in energy demand during warmer months.

Table 9. Comparison of carbon emissions intensity (kg CO₂/m²) between the base model without a green wall and the enhanced model after installing the green walls.

Date	End Uses	Before Installing the Green Wall	After Installing the Green Wall
12 January	Heating	0.495	0.518
	Interior Lighting	0.011	0.011
	Electric Equipment	0.018	0.017
	Pumps	0	0
	Water Systems	0.003	0.003
	cei	0.527	0.549
29 March	Heating	0.025	0.041
	Cooling	0.028	0.002
	Interior Lighting	0.019	0.019
	Electric Equipment	0.031	0.031
	Water Systems	0.005	0.005
	cei	0.108	0.098
29 July	Cooling	0.085	0.054
	Interior Lighting	0.003	0.003
	Electric Equipment	0.010	0.010
	Water Systems	0.002	0.002
	cei	0.100	0.069
15 October	Heating	0.012	0.022
	Interior Lighting	0.001	0.001
	Electric Equipment	0.008	0.008
	Water Systems	0.001	0.001
	cooling	0	0
	cei	0.022	0.032

4. Discussion

The implementation of VGSs in urban environments reveals complex and sometimes contradictory effects on microclimate parameters and building energy performance. This study's findings both challenge and confirm existing understanding of green wall performance in urban settings.

The extant literature suggests that the introduction of VGSs would result in positive cooling effects through transpiration and evaporative processes. Our results indicate minimal reductions in air temperature, and, in some cases, some similarities can be detected compared to several prominent studies in the literature. A distinguishing feature of our research is the examination of a more expansive urban area, encompassing complete facade coverage, in contrast to the smaller-scale studies and diverse typologies of vertical greenery systems and climate zones that are frequently focused on in the existing literature.

Air temperature changes, ranging from −1.6 °C to 1.3 °C, depending on the season and simulation period, show the insignificant cooling effect of green walls on outdoor air temperature and some exceptions when the heating effect occurred on several occasions [36], especially in summer. Similarly, [37] provided insignificant reduction in air temperature, ranging from −1.17 °C to −0.09 °C after the installation of LWs in different climate zones

(Cfb). The cooling effect of green walls can be comprehended as well in a semi-arid climate zone (BWh) with double the thickness in the substrate. However, the range was much greater with a maximum reduction of 10 °C [39]. However, the results are partly aligned with the previous study [27] being conducted in the same study area, with the difference between the typology of the VGSs, lower substrate thickness, and coverage area. This would provide additional information that, in the same area, even with different types of LWs, increasing the greenery coverage area would result in better cooling performance [31,55].

In addition to air temperature, the results also highlight reductions in T_{mrt} and outdoor thermal comfort indices [37]. Considering the effect of wall albedo configuration after introducing green walls as low-albedo surfaces with leaf and soil reflection values of 0.22 and 0.3, the findings showed better cooling effects on air temperature compared to the findings of [20]. Their study concluded that changing the albedo of the wall does not significantly improve air temperature and suggested evaporative cooling as a more effective strategy. In this context, the green walls, despite having low albedo, demonstrated enhanced cooling through the evaporative cooling effect provided by vegetation, aligning with their recommendations. Furthermore, the extant literature has explored the effect of surface albedo on localized T_{mrt} . Research findings indicate that modifying solely the albedo of vertical surfaces with inherently low albedo values frequently results in deterioration of the T_{mrt} reduction effect. The findings indicate that medium albedo walls (0.4) would have a better mean delta T_{mrt} reduction of -1.5 °C, which is superior to that of low albedo walls (0.1). The mean delta T_{mrt} reduction was found to be -0.8 °C [20], and in some cases, there was an increase in temperature, with values ranging from 1.8 °C to 3.5 °C during winter and from 2 °C to 4 °C during summer in all the climates under study [52]. However, our findings demonstrated that green walls, even with low albedo, would effectively improve T_{mrt} [20,52]. Our findings directly reflect the expected improvement in thermal comfort mentioned in the introduction, where green infrastructure is suggested to reduce the UTCI by mitigating heat exposure. The reduction in UTCI values indicates the effectiveness of green wall thermal properties in alleviating thermal stress as a mitigation strategy that can locally counteract the effects of climate change. The decrease in T_{mrt} and UTCI under current climate conditions during summer, particularly during the hours around noon, is also consistent with the literature [36], which suggests that green walls can lower T_{mrt} by blocking direct solar radiation and increasing local shading. UTCI values also showed similar improvement with the green walls in place.

Our findings are significantly consistent with theories about urban canyon effects on thermal performance. Studies like [14] identify SVF as a primary contributor to urban heat island intensity, suggesting that moderate-to-high SVF can mitigate UHI, whereas extremely high SVF levels intensify it, where in some studies the cooling effects of VGSs on air temperature were greater in central canyons [31]. Similarly, our results demonstrate that these areas show enhanced cooling benefits from green walls, with T_{mrt} reductions and outdoor comfort improvements greater than in open areas [16]. This challenges current urban design paradigms and suggests that VGSs might be particularly valuable in dense urban environments previously considered challenging for thermal management.

Results from [38] show almost a 29% reduction in annual carbon emissions can be expected [33]. Also concluded that greenery systems such as green roofs and trees would cause a reduction even in the energy performance of the buildings, which consequently results in the reduction in (cei). In our study, (cei) reduction ranges from 9% to 31% for spring and summer, although there was some increase in autumn and winter of 4% and 45%.

Our studies have shown that green walls have a significant impact on energy efficiency, especially in warm seasons. However, climate change may exacerbate or moderate these effects. Rising temperatures and the occurrence of heat waves in the future will double the

importance of the cooling role of green walls, as this mitigation strategy can help reduce the urban heat island effect and increase thermal comfort. On the other hand, in cold seasons, climate change may cause changes in energy consumption patterns. A decrease in cold days or changes in the intensity of winter colds can reduce the negative impact of green walls on energy consumption. For this reason, the design and implementation of greenery systems must be adapted to future climate conditions and possible temperature changes to increase energy efficiency and control carbon dioxide emissions.

5. Limitation

In the context of outdoor comfort analysis, there exists a paucity of modeling tools that can predict microclimatic parameters, including air temperature and T_{mrt} . The predominant and widely utilized methods and software for calculating T_{mrt} are ENVI-met and Ladybug Tools. These tools are designed to calculate radiation components, including direct, diffuse, and reflected shortwave and longwave radiation from surfaces. Notably, both tools incorporate the calculation of longwave radiation from the sky. Both tools incorporate view factors, with Ladybug Tools utilizing ray-tracing and Envi-met employing Indexed View Sphere (IVS) methods. A distinguishing feature of both tools is their capacity to model radiation exchange between buildings, vegetation, and surface temperatures, which is a critical input parameter for T_{mrt} calculation. The primary distinction between the two tools lies in their approach to wind profiles. Envi-met utilizes a 3D computational fluid dynamics (CFD) model, a technique that has proven to be highly effective in simulating convective cooling or warming caused by wind. In contrast, Ladybug Tools utilize weather station wind data from EPW files, similar to the approach employed in this study, or the Butterfly plug-in, which employs CFD simulations utilizing the OpenFOAM framework. Ladybug Tools effectively models vegetation by simulating evapotranspiration, radiation exchanges, and thermal properties. However, these tools have limitations, as they treat vegetation properties as static, such as plant height and leaf area index (LAI). Furthermore, the potential impact of central area pollution on solar radiation magnitude was not considered in this study, as the weather data were obtained from the Turin-Caselle Airport station, which is situated in a rural environment.

6. Conclusions

This study underscores the considerable potential of VGSs, particularly green walls, in mitigating UHI effects and enhancing urban microclimates under both current and future climate scenarios. While the reductions in outdoor air temperature were modest, with variations ranging from $-1.6\text{ }^{\circ}\text{C}$ to $1.3\text{ }^{\circ}\text{C}$, the impact on T_{mrt} was more pronounced, with reductions reaching up to $-2.27\text{ }^{\circ}\text{C}$ during peak solar radiation in summer periods. These improvements were most evident in urban canyons and areas with low SVF, thereby demonstrating the capacity of green walls to improve thermal comfort in densely populated urban environments. The UTCI also showed consistent improvements, with maximum reductions of $0.55\text{ }^{\circ}\text{C}$ under future climate projections for 2050 at noon in summer. Green walls proved particularly effective during summer, reducing cooling demand and lowering (cei) by up to 31%. However, during winter, a slight increase in heating demand led to higher emissions, underscoring the importance of optimizing green wall designs for seasonal energy performance. The findings indicate that the effectiveness of green walls is contingent on factors such as building orientation, solar exposure, and local urban morphology. Ensuring sufficient sunlight for vegetation is imperative for sustaining growth and optimizing the cooling effects driven by evapotranspiration. In the context of projected climate change, green walls are poised to play a pivotal role in adapting urban environments to rising temperatures and increasingly frequent heat waves.

While the present study did not examine partial coverage, this is an intriguing area for future research. The optimization of the model to achieve comparable performance with reduced coverage ratios could significantly increase its practicality. Furthermore, advancements in this field could include the incorporation of locally adapted plant species, leveraging their distinctive thermal characteristics to enhance cooling efficiency, and adapting to diverse climatic and urban conditions.

In summary, the integration of green walls emerges as a pragmatic and sustainable approach to enhance outdoor thermal comfort, curtail carbon emissions, and mitigate Urban Heat Island (UHI) effects, particularly within urban contexts characterized by densely developed environments. These findings provide a solid foundation for integrating green walls into comprehensive urban climate adaptation strategies.

Author Contributions: Conceptualization, A.D.L.; methodology, A.D.L. and S.M.H.; software, A.D.L. and S.M.H.; validation, A.D.L. and S.M.H.; formal analysis, A.D.L. and S.M.H.; investigation, A.D.L.; data curation, A.D.L. and M.H.; writing—original draft preparation, A.D.L.; writing—review and editing, S.M.H., M.H., P.D. and F.S.; visualization, A.D.L. and S.M.H.; supervision, S.M.H. and P.D. All authors have read and agreed to the published version of the manuscript.

Funding: This research received no external funding.

Data Availability Statement: The data used to support the findings of this study can be made available by the corresponding author upon request.

Acknowledgments: We would like to acknowledge that this study is part of our contribution to the project titled: “EUDP 2023-I Deltagelse i IEASHC 70 Low Carbon, High Comfort Integrated Lighting”. Also, this work is part of the research activity developed by the authors within the framework of the “PNRR”: SPOKE 7 “CCAM, Connected Networks, and Smart Infrastructure”-WP4.

Conflicts of Interest: The authors declare no conflict of interest.

Abbreviations

The following abbreviations are used in this manuscript:

BT	Brightness Temperature
cei	Carbon Emission Intensity
CFD	Computational Fluid Dynamics
CVRMSE	Cumulative Variation of Root Mean Squared Error
EGR	Extensive Green Roof
ERF	Effective Radiant Field
GWs	Green Wall
HS	Heavy Systems
HVAC	Heating, Ventilation, and Air Conditioning
LAI	Leaf Area Index
LS	Light Systems
LST	Last Surface Temperature
MBE	Mean Bias Error
MV	Mur Vegetal
MWh	Megawatt Hour
NDVI	Normalized Different Vegetation Index
NIR	Near-infrared
PET	Physiological Equivalent Temperature
SL	Street Length
SUHI	Surface Urban Heat Island
SVF	Sky View Factor
TIR	Thermal Infrared
Tmrt	Mean Radiant Temperature

TMY	Typical Meteorological Year
UHI	Urban Heat Island
UTCI	Universal Thermal Climate Index
UWG	Urban Weather Generator
VGSs	Vertical Greenery Systems

Nomenclature

a_{lw}	Long wave absorptivity/emissivity (clothing) default 0.95
A_p/AD	The projection factor is determined through a look-up table available at ASHRAE and is determined by solar altitude, solar azimuth, and the body's related angle.
a_{sw}	Short wave absorptivity of the person (skin and clothing) default 0.7
f_{bes}	Fraction of body exposed to direct solar radiation
f_{eff}	Fraction of the body that can radiate heat (related to posture)
f_{svv}	Sky view factor
h_r	Radiant heat transfer coefficient
I_{diff}	Diffuse radiation (W/m^2)
I_{dir}	Direct radiation (W/m^2)
I_{th}	Global horizontal radiation (W/m^2)
R_{floor}	Ground reflectance
F_i	View factors to each surface
P_v	Proportion of Vegetation
T_a	Dry bulb temperature
T_i	Surface temperature
AL	Band-Specific Additive Rescaling Factor
C	Stephan–Boltzmann constant
σ	Stefan Boltzmann constant (5.667×10^{-8})
H	Planck constant
H/W	Aspect ratio
L λ	Total spectral radiance
ML	Band-specific multiplicative rescaling factor
Qcal	Band 10
TOA	Top of Atmospheric
ϵ	Land surface emissivity
λ	Emitted radiance
c	Light velocity
ϵ_{person}	The emissivity of the human (assumed to be 0.95)

Appendix A

High-precision meteorological data Table A1 was used to validate the simulation results, allowing for reliable comparisons between observed environmental conditions and model predictions.

Table A1. Insite measurements sensors characteristics.

Wind Vane Anemometer DV20	
Anodized aluminum weathervane/Long-life potentiometric transducer	
Measuring range	0°–360°
Resolution	0.35° for the system
Precision	±2.8°
Operating temperature	0 °C–+60 °C; –30–+60 °C with electric heater
Dimensions	561 × 406 (mm)
Weight	0.9 (kg)

Table A1. Cont.

Tachometer Anemometer Vv20	
Three-blade polycarbonate reel/solid-state measuring transducer with frequency output	
Safety field	0–220 (km/h), 61 (m/s)
Resolution	0.06 (m/s), 0.2 (km/h)
Sensitivity	less than 0.02 (m/s), threshold of 1.8 (km/h), 0.5 (m/s)
Precision	±0.25 (km/h), 0.07 (m/s) or 1% of reading
Operating temperature	from −30 °C to +60 °C (with heater)
Dimensions	178 (Ø) × 281 (mm)
Weight	0.9 (kg)
Support Arm BSA20	
Made entirely of stainless steel/Comes complete with cables and connectors for sensors	
Dimensions	1490 × 790 (mm)
Weight	6.5 (kg) (including sensors)
Lightning rod made of stainless steel	1700 (mm) long/10 (mm) in diameter
Pyranometer HE20K	
Measuring range	0–1500 (W/m ²)
Spherical window	305–2800 (nm)
Non-linearity	±1.5% in the range 0–1000 (W/m ²)
Operating temperature range	−40 + 60 °C
Precision	5% (daily total), 1st class WMO (ISO 9060)
Influencing factors	sensitivity dependence on temperature < 2% in the range from −10 °C to +40 °C
Dimensions	150 (Ø) × 115 (mm)
Weight	1 (kg) (with shield)
THS Thermo-Hygrometer	
Hygrometer—Measurement range	0 to 100% RH
HYGROMETER—Temperature range	−50–+100 °C
SHIELDED AIR THERMOMETER—Sensing element	PT100 1/3 Din Class A
HYGROMETER—Accuracy	±1.5% from 0 to 100% RH
SHIELDED AIR THERMOMETER—Measurement range	−50–+100 °C
SHIELDED AIR THERMOMETER—Accuracy at 23 °C	±0.2 °C
PG10 and PG10R	
Connection with Data-logger	Interface RS-485 with SDI-12 protocol
Measurement Range	up to 1000 (mm/h)
Output Resolution	0.1 (mm)
Collecting Area	1000 (cm ²)
Accuracy	Max 3% < 800 (mm/h), Max 5%, 800–1000 (mm/h)
Temperature Range	PG10: 32 °F/140 °F, 0 °C/60 °C, PG10R: −22 °F/140 °F, −30 °C/60 °C
Sensor Type	Tipping bucket rain gauge

Appendix B

Figure A1 compares the levels of direct solar radiation recorded in the EPW weather file under current conditions and future projections in 2050. It shows how the intensity and distribution of solar radiation change over time and provides valuable context for understanding future climate scenarios.

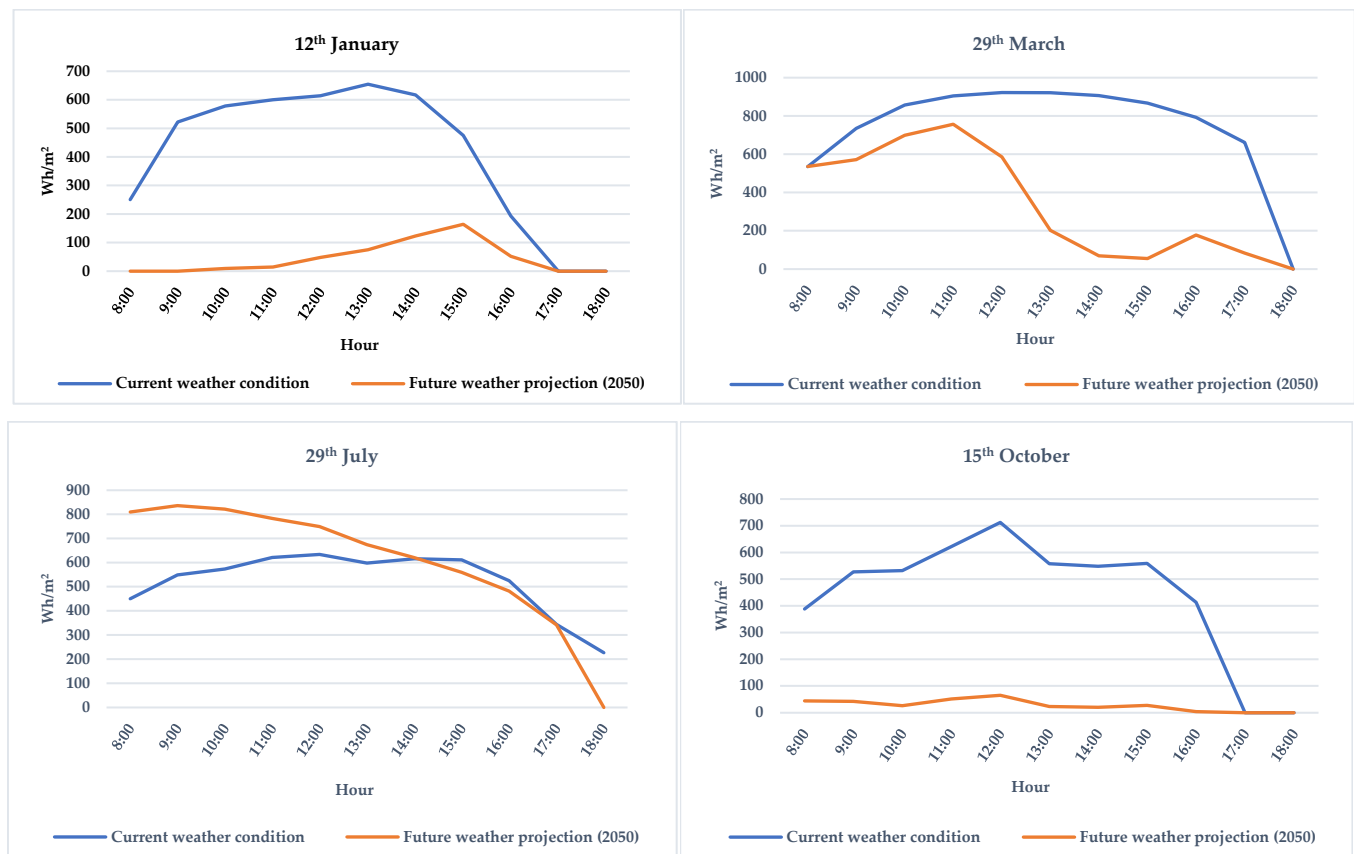


Figure A1. Direct solar radiation under current weather conditions and 2050 projection, based on data from the original EPW file.

References

1. United Nations, D. of E. and S.A.P.D. World Urbanization Prospects: The 2014 Revision; New York, 2015. 2015. Available online: <https://population.un.org/wup/assets/WUP2014-Report.pdf> (accessed on 20 December 2024).
2. Ng, E.; Chen, L.; Wang, Y.; Yuan, C. A Study on the Cooling Effects of Greening in a High-Density City: An Experience from Hong Kong. *Build. Environ.* **2012**, *47*, 256–271. [[CrossRef](#)]
3. De Groeve, M.; Kale, E.; Godts, S.; Orr, S.A.; De Kock, T. Impact of Vertical Greening on Urban Microclimate and Historic Building Materials: A Meta-Analysis. *Build. Environ.* **2024**, *253*, 111365. [[CrossRef](#)]
4. Boccalatte, A.; Fossa, M.; Thebault, M.; Ramousse, J.; Ménézo, C. Mapping the Urban Heat Island at the Territory Scale: An Unsupervised Learning Approach for Urban Planning Applied to the Canton of Geneva. *Sustain. Cities Soc.* **2023**, *96*, 104677. [[CrossRef](#)]
5. Cheval, S.; Amihăesei, V.-A.; Chitu, Z.; Dumitrescu, A.; Falcescu, V.; Iraşoc, A.; Micu, D.M.; Mihulet, E.; Ontel, I.; Paraschiv, M.-G.; et al. A Systematic Review of Urban Heat Island and Heat Waves Research (1991–2022). *Clim. Risk Manag.* **2024**, *44*, 100603. [[CrossRef](#)]
6. Schmidt, V. Urban Morphology as a Key Parameter for Mitigating Urban Heat?—A Literature Review. *IOP Conf. Ser. Earth Environ. Sci.* **2024**, *1363*, 012074. [[CrossRef](#)]
7. Zheng, Y.; Ren, C.; Shi, Y.; Yim, S.H.L.; Lai, D.Y.F.; Xu, Y.; Fang, C.; Li, W. Mapping the Spatial Distribution of Nocturnal Urban Heat Island Based on Local Climate Zone Framework. *Build. Environ.* **2023**, *234*, 110197. [[CrossRef](#)]
8. Eslamirad, N.; Sepúlveda, A.; De Luca, F.; Sakari Lylykangas, K.; Ben Yahia, S. Outdoor Thermal Comfort Optimization in a Cold Climate to Mitigate the Level of Urban Heat Island in an Urban Area. *Energies* **2023**, *16*, 4546. [[CrossRef](#)]
9. Gholami, H.; Kamelnia, H.; Mahdavinjad, M.J.; Sangin, H. Optimizing Building Configuration and Orientation for Social Housing Projects in Iran. *Iran. J. Energy Environ.* **2025**, *16*, 289–308. [[CrossRef](#)]
10. Rabie, S.; Sangin, H.; Zandieh, M. The Orientation of Village, the Most Important Factor in Rural Sustainability in Cold Climate (Case Study: Masuleh and Uramantakht). *J. Sol. Energy Res.* **2021**, *6*, 761–776. [[CrossRef](#)]
11. Shao, L.; Liao, W.; Li, P.; Luo, M.; Xiong, X.; Liu, X. Drivers of Global Surface Urban Heat Islands: Surface Property, Climate Background, and 2D/3D Urban Morphologies. *Build. Environ.* **2023**, *242*, 110581. [[CrossRef](#)]

12. Lin, T.-P.; Matzarakis, A.; Hwang, R.-L. Shading Effect on Long-Term Outdoor Thermal Comfort. *Build. Environ.* **2010**, *45*, 213–221. [[CrossRef](#)]
13. Oke, T.R. *Boundary Layer Climates*; Routledge: London, UK, 2002; ISBN 0-203-71545-4.
14. Güller, C.; Toy, S. The Impacts of Urban Morphology on Urban Heat Islands in Housing Areas: The Case of Erzurum, Turkey. *Sustainability* **2024**, *16*, 791. [[CrossRef](#)]
15. Ahmadi Venhari, A.; Tenpierik, M.; Taleghani, M. The Role of Sky View Factor and Urban Street Greenery in Human Thermal Comfort and Heat Stress in a Desert Climate. *J. Arid Environ.* **2019**, *166*, 68–76. [[CrossRef](#)]
16. Fang, Z.; He, H.; Mao, Y.; Feng, X.; Zheng, Z.; Guo, Z. Investigating an Accurate Method for Measuring the Outdoor Mean Radiation Temperature. *Int. J. Therm. Sci.* **2023**, *188*, 108219. [[CrossRef](#)]
17. Azimi, Z.; Shafaat, A. Proposing Design Strategies for Contemporary Courtyards Based on Thermal Comfort in Cold and Semi-Arid Climate Zones. *Build. Environ.* **2024**, *266*, 112150. [[CrossRef](#)]
18. Li, J.; Wang, J.; Wong, N.H. Urban Micro-Climate Research in High Density Cities: Case Study in Nanjing. *Procedia Eng.* **2016**, *169*, 88–99. [[CrossRef](#)]
19. Irfeey, A.M.M.; Chau, H.-W.; Sumaiya, M.M.F.; Wai, C.Y.; Muttill, N.; Jamei, E. Sustainable Mitigation Strategies for Urban Heat Island Effects in Urban Areas. *Sustainability* **2023**, *15*, 10767. [[CrossRef](#)]
20. Lopez-Cabeza, V.P.; Alzate-Gaviria, S.; Diz-Mellado, E.; Rivera-Gomez, C.; Galan-Marin, C. Albedo Influence on the Microclimate and Thermal Comfort of Courtyards under Mediterranean Hot Summer Climate Conditions. *Sustain. Cities Soc.* **2022**, *81*, 103872. [[CrossRef](#)]
21. Morakinyo, T.E.; Lam, Y.F. Simulation Study on the Impact of Tree-Configuration, Planting Pattern and Wind Condition on Street-Canyon's Micro-Climate and Thermal Comfort. *Build. Environ.* **2016**, *103*, 262–275. [[CrossRef](#)]
22. Cortês, A.S.B.; Almeida, J.A.S.; Kanoun-Boulé, M.; Tadeu, A. Green Facades and Living Walls: The Portuguese Experience. In *INCREaSE*; Springer International Publishing: Cham, Switzerland, 2018; pp. 562–570; ISBN 978-3-319-70271-1.
23. Zaina, S.M.; Fadli, F.; Hosseini, S.M. Evaluation of Smart Irrigation Systems in Hot-Arid Climates for Green Roofs and Walls: Case of Doha, Qatar. *Smart Sustain. Built Environ.* **2022**, *11*, 346–367. [[CrossRef](#)]
24. Ramadhan, A.M.; Mahmoud, A.H. Evaluating the Efficiency of a Living Wall Facade as a Sustainable Energy-Saving Alternative in Hot Arid Regions. *J. Eng. Appl. Sci.* **2023**, *70*, 96. [[CrossRef](#)]
25. Reynolds, H.L.; Brandt, L.; Fischer, B.C.; Hardiman, B.S.; Moxley, D.J.; Sandweiss, E.; Speer, J.H.; Fei, S. Implications of Climate Change for Managing Urban Green Infrastructure: An Indiana, US Case Study. *Clim. Change* **2020**, *163*, 1967–1984. [[CrossRef](#)]
26. Sommese, F. Nature-Based Solutions to Enhance Urban Resilience in the Climate Change and Post-Pandemic Era: A Taxonomy for the Built Environment. *Buildings* **2024**, *14*, 2190. [[CrossRef](#)]
27. Susca, T.; Zanghirella, F.; Del Fatto, V. Building Integrated Vegetation Effect on Micro-Climate Conditions for Urban Heat Island Adaptation. Lesson Learned from Turin and Rome Case Studies. *Energy Build.* **2023**, *295*, 113233. [[CrossRef](#)]
28. Wang, P.; Wong, Y.H.; Tan, C.Y.; Li, S.; Chong, W.T. Vertical Greening Systems: Technological Benefits, Progresses and Prospects. *Sustainability* **2022**, *14*, 12997. [[CrossRef](#)]
29. Zhang, L.; Deng, Z.; Liang, L.; Zhang, Y.; Meng, Q.; Wang, J.; Santamouris, M. Thermal Behavior of a Vertical Green Facade and Its Impact on the Indoor and Outdoor Thermal Environment. *Energy Build.* **2019**, *204*, 109502. [[CrossRef](#)]
30. Larsen, S.F.; Filippin, C.; Lesino, G. Thermal Simulation of a Double Skin Façade with Plants. *Energy Procedia* **2014**, *57*, 1763–1772. [[CrossRef](#)]
31. Herath, H.M.P.I.K.; Halwatura, R.U.; Jayasinghe, G.Y. Modeling a Tropical Urban Context with Green Walls and Green Roofs as an Urban Heat Island Adaptation Strategy. *Procedia Eng.* **2018**, *212*, 691–698. [[CrossRef](#)]
32. Mutani, G.; Todeschi, V. The Effects of Green Roofs on Outdoor Thermal Comfort, Urban Heat Island Mitigation and Energy Savings. *Atmosphere* **2020**, *11*, 123. [[CrossRef](#)]
33. Ciacci, C.; Banti, N.; Di Naso, V.; Bazzocchi, F. Green Strategies for Improving Urban Microclimate and Air Quality: A Case Study of an Italian Industrial District and Facility. *Build. Environ.* **2023**, *244*, 110762. [[CrossRef](#)]
34. Kim, E.S.; Yun, S.H.; Lee, D.K.; Kim, N.Y.; Piao, Z.G.; Kim, S.H.; Park, S. Quantifying Outdoor Cooling Effects of Vertical Greening System on Mean Radiant Temperature. *Dev. Built Environ.* **2023**, *15*, 100211. [[CrossRef](#)]
35. Djedjig, R.; Belarbi, R.; Bozonnet, E. Green Wall Impacts inside and Outside Buildings: Experimental Study. *Energy Procedia* **2017**, *139*, 578–583. [[CrossRef](#)]
36. Zuckerman, N.; Shiloah, N.; Lensky, I.M. Quantifying the Impact of Vertical Greenery Systems (VGS) on Mediterranean Urban Microclimate during Heat Wave Events. *Build. Environ.* **2025**, *267*, 112151. [[CrossRef](#)]
37. Taher, H.; Elsharkawy, H.; Rashed, H.F. Urban Green Systems for Improving Pedestrian Thermal Comfort and Walkability in Future Climate Scenarios in London. *Buildings* **2024**, *14*, 651. [[CrossRef](#)]
38. Nashaat, B. Optimizing Parametric Green Facades for Daylighting and Thermal Comfort in Egypt's Hot Climates. *Port Said Eng. Res. J.* **2024**, *28*, 72–83. [[CrossRef](#)]

39. Wahba, S.; Kamil, B.; Nassar, K.; Abdelsalam, A. Green Envelop Impact on Reducing Air Temperature and Enhancing Outdoor Thermal Comfort in Arid Climates. *Civil Eng. J.* **2019**, *5*, 1124–1135. [[CrossRef](#)]
40. U.S.G. Survey. Available online: <https://earthexplorer.usgs.gov/> (accessed on 12 July 2024).
41. Ladybug Tools EPW Map. Available online: <https://www.ladybug.tools/epwmap/> (accessed on 8 March 2024).
42. Agenzia Regionale per la Protezione Ambientale (ARPA) Piemonte di Torino Hourly Meteorological and Hydrological Data. Available online: <https://www.arpa.piemonte.it/> (accessed on 2 May 2024).
43. Machard, A.; Salvati, A.; Tootkaboni, P.M.; Gaur, A.; Zou, J.; Wang, L.L.; Baba, F.; Ge, H.; Bre, F.; Bozonnet, E.; et al. Typical and Extreme Weather Datasets for Studying the Resilience of Buildings to Climate Change and Heatwaves. *Sci. Data* **2024**, *11*, 531. [[CrossRef](#)]
44. Heiranipour, M.; Favoino, F.; Juaristi Gutierrez, M.; Avesani, S. *Typical and Extreme (Heatwave) Future Weather for Building Energy Simulations: Case for Turin and Bolzano, Italy, and De Bilt, Netherlands*; Zenodo: Genève, Switzerland, 2024.
45. Boccardo, P.; Giulio Tonolo, F. Remote Sensing Role in Emergency Mapping for Disaster Response. In *Engineering Geology for Society and Territory*; Springer International Publishing: Cham, Switzerland, 2015; Volume 5, pp. 17–24.
46. Avdan, U.; Jovanovska, G. Algorithm for Automated Mapping of Land Surface Temperature Using LANDSAT 8 Satellite Data. *J. Sens.* **2016**, *2016*, 1–8. [[CrossRef](#)]
47. Kasniza Jumari, N.A.S.; Ahmed, A.N.; Huang, Y.F.; Ng, J.L.; Koo, C.H.; Chong, K.L.; Sherif, M.; Elshafie, A. Analysis of Urban Heat Islands with Landsat Satellite Images and GIS in Kuala Lumpur Metropolitan City. *Heliyon* **2023**, *9*, e18424. [[CrossRef](#)]
48. Rahman, M.N.; Rony, M.R.H.; Jannat, F.A.; Chandra Pal, S.; Islam, M.S.; Alam, E.; Islam, A.R.M.T. Impact of Urbanization on Urban Heat Island Intensity in Major Districts of Bangladesh Using Remote Sensing and Geo-Spatial Tools. *Climate* **2022**, *10*, 3. [[CrossRef](#)]
49. Dabove, P.; Daud, M.; Olivotto, L. Revolutionizing Urban Mapping: Deep Learning and Data Fusion Strategies for Accurate Building Footprint Segmentation. *Sci. Rep.* **2024**, *14*, 13510. [[CrossRef](#)] [[PubMed](#)]
50. Regione Piemonte Geo Piemonte. Available online: <https://geoportale.igr.piemonte.it/cms/> (accessed on 31 March 2024).
51. Rezaei, F.; Sangin, H.; Heiranipour, M.; Attia, S. A Multi-Objective Optimization of Window and Light Shelf Design in Office Buildings to Improve Occupants' Thermal and Visual Comfort. *J. Daylighting* **2024**, *11*, 55–68. [[CrossRef](#)]
52. Naboni, E.; Milella, A.; Vadalà, R.; Fiorito, F. On the Localised Climate Change Mitigation Potential of Building Facades. *Energy Build.* **2020**, *224*, 110284. [[CrossRef](#)]
53. Mackey, C.; Galanos, T.; Norford, L.; Sadeghipour Roudsari, M. Wind, Sun, Surface Temperature, and Heat Island: Critical Variables for High-Resolution Outdoor Thermal Comfort. In *Proceedings of the Building Simulation 2017: 15th Conference of IBPSA*, 7 August 2017; IBPSA: San Francisco, CA, USA; pp. 985–993.
54. Salvati, A.; Kolokotroni, M. Urban Microclimate and Climate Change Impact on the Thermal Performance and Ventilation of Multi-Family Residential Buildings. *Energy Build.* **2023**, *294*, 113224. [[CrossRef](#)]
55. Dardir, M.; Berardi, U. Development of Microclimate Modeling for Enhancing Neighborhood Thermal Performance through Urban Greenery Cover. *Energy Build.* **2021**, *252*, 111428. [[CrossRef](#)]
56. Naboni, E.; Meloni, M.; Mackey, C.; Kaempfer, J. The Simulation of Mean Radiant Temperature in Outdoor Conditions: A Review of Software Tools Capabilities. In *Proceedings of Building Simulation 2019: 16th Conference of IBPSA*, Rome, Italy, 2–4 September 2019; pp. 3234–3241.
57. Bueno, B.; Norford, L.; Hidalgo, J.; Pigeon, G. Prediction of the Urban Heat Island Effect to Be Used in Building Energy Analyses. In *Proceedings of the SimBuild Conference 2012: 5th Conference of IBPSA USA*, Madison, WI, USA, 1–3 August 2012; Volume 5, pp. 236–245.
58. Arens, E.; Hoyt, T.; Zhou, X.; Huang, L.; Zhang, H.; Schiavon, S. Modeling the Comfort Effects of Short-Wave Solar Radiation Indoors. *Build. Environ.* **2015**, *88*, 3–9. [[CrossRef](#)]
59. American Society of Heating, Refrigerating, and Air-Conditioning Engineers. *Measurement of Energy, Demand, and Water Savings*. In *Ashrae Guideline 14-2014: Measurement of Energy, Demand and Water Savings*; American Society of Heating, Refrigerating, and Air-Conditioning Engineers: Peachtree Corners, GA, USA, 2014.
60. (NREL), N.R.E.L. EnergyPlus™ 2017.
61. Arengi, A.; Perra, C.; Caffi, M. Simulating and Comparing Different Vertical Greenery Systems Grouped into Categories Using EnergyPlus. *Appl. Sci.* **2021**, *11*, 4802. [[CrossRef](#)]
62. Hosseini, S.M.; Heiranipour, M.; Wang, J.; Hinkle, L.E.; Triantafyllidis, G.; Attia, S. Enhancing Visual Comfort and Energy Efficiency in Office Lighting Using Parametric-Generative Design Approach for Interactive Kinetic Louvers. *J. Daylighting* **2024**, *11*, 69–96. [[CrossRef](#)]

-
63. Stec, W.J.; Paassen, A.H.C. van Symbiosis of the Double Skin Façade with the HVAC System. *Energy Build.* **2005**, *37*, 461–469. [[CrossRef](#)]
 64. The International Energy Agency (IEA) Greenhouse Gas Emissions from Energy Data Explorer. Available online: <https://www.iea.org> (accessed on 16 December 2024).

Disclaimer/Publisher’s Note: The statements, opinions and data contained in all publications are solely those of the individual author(s) and contributor(s) and not of MDPI and/or the editor(s). MDPI and/or the editor(s) disclaim responsibility for any injury to people or property resulting from any ideas, methods, instructions or products referred to in the content.